

Evaluating backreaction with the ellipsoidal collapse model

Francesco Montanari and Syksy Räsänen

University of Helsinki, Department of Physics
and Helsinki Institute of Physics
P.O. Box 64, FIN-00014 University of Helsinki, Finland

E-mail: syksy.rasanen@iki.fi, francesco.montanari@helsinki.fi

Abstract. We evaluate the effect of structure formation on the average expansion rate with a statistical treatment where density peaks and troughs are modelled as homogeneous ellipsoids. This extends earlier work that used spherical regions. We find that the shear and the presence of filamentary and planar structures have only a small impact on the results. The expansion rate times the age of the universe Ht increases from $2/3$ to 0.83 at late times, in order of magnitude agreement with observations, although the change is slower and takes longer than in the real universe. We discuss shortcomings that have to be addressed for this and similar statistical models in the literature to develop into realistic quantitative treatment of backreaction.

Contents

1	Introduction	1
2	Average quantities and homogeneous ellipsoids	2
2.1	Backreaction	2
2.2	Evolution of homogeneous ellipsoids	3
2.3	The average expansion rate	6
3	Results	8
3.1	The average expansion rate	8
3.2	The shear	11
4	Discussion	16
5	Conclusions	20

1 Introduction

Evaluating backreaction. There is much observational evidence that the universe is statistically homogeneous and isotropic, with a homogeneity scale of the order 100 Mpc [1–5]. However, this does not imply that the average expansion rate necessarily obeys the Friedmann–Robertson–Walker (FRW) equations, which describe a universe that is exactly homogeneous and isotropic. The effect of clumpiness on average evolution is called backreaction [6–9]. It has been suggested that backreaction could explain the late-time cosmic acceleration [10–13]. In Newtonian gravity backreaction reduces to a boundary term [14]. In general relativity this is not the case [10], but the average expansion rate (though not necessarily the luminosity distance [15]) is nevertheless close to its FRW value if the metric is close to the FRW metric [8] (see [16] for a related debate). However, it is difficult to estimate the effect in general relativity without assuming that the metric is everywhere close to the same global FRW metric. It has been shown with an exact toy model that structures can have a large effect on the expansion rate and light propagation, even when they are small and the universe is statistically homogeneous and isotropic [17], but the magnitude of the effect in the real universe remains unclear.

The problem can be approached in two ways. First, without calculating the effect of structures on the expansion rate, it is possible to formulate consistency tests of the FRW metric [18–20] and compare them to observations [20, 21]. Observations can also be used to test backreaction [17, 22], given a relation between the average expansion rate and light propagation [17, 23–26]. Second, we can try to evaluate the effect of the non-linear structures on the expansion rate, either by constructing exact or statistical analytical models (such as models with discrete matter [27, 28] and models using data from Newtonian N -body simulations [29]), or via relativistic cosmological simulations, some of which are in the weak field regime [30] (where the effect is known to be small) but others are fully non-linear [31] and cosmological [32].

In [33] a statistical model was considered, with structures taken to form on peaks and troughs of the initial density field, leading to a distribution of collapsing regions and underdense voids. (This is a simplified picture, not all non-linear structures in the real universe are

associated with extrema of the density field [34–39].) The environment of the extrema was modelled with the Newtonian spherical collapse model and its underdense equivalent. This treatment misses anisotropic structures such as filaments and sheets, which are prevalent features of the real universe [40, 41]. A related shortcoming, noted in [33], is the absence of internal and external tidal effects, i.e. angular shear [34, 42–52], which can potentially have a large effect on the average expansion rate. Deviations from spherical symmetry have been found to be important for the calculation of the mass function and expansion rate of collapsing objects [53–63]. Mass function calculations are concerned with the distribution of stabilised structures, not the details of the formation process. For backreaction, the opposite is true: the endpoint of structure formation is (at least for collapsing objects) less interesting than the evolution between the linear regime and the final stage.

We extend the calculation of [33], using a Newtonian ellipsoidal model for the structures. For spherically symmetric dust, the average expansion rate is independent of the radial density profile in Newtonian gravity [64], though not in general relativity [17, 65, 66]. So the Newtonian spherical model covers arbitrary inhomogeneity without anisotropy. In contrast, in order to be tractable, the ellipsoidal model has to be homogeneous, but allows for anisotropy. (Indeed, “homogeneous anisotropic model” might be a more appropriate name.) In this sense, the ellipsoidal model can be seen as a different approximation than the spherical model, not a generalisation of it, although the expansion rate of the spherical case is a subcase of ellipsoidal expansion. In the context of peaks and troughs, the ellipsoidal model can be thought of as the leading approximation in a series expansion of the gravitational potential around an extremum [50].

In section 2 we give the details of the ellipsoidal collapse model and the ensemble averaging that we use. In section 3 we give the results for the expansion rate and compare to the spherical case, and consider shear and filamentary and planar structures. In section 4 we discuss the results and how the calculation and similar approaches in the literature would have to be improved in order to go from toy models to realistic quantitative descriptions. In section 5 we summarise our conclusions.

2 Average quantities and homogeneous ellipsoids

2.1 Backreaction

The Buchert equations. Assuming that matter consists of irrotational dust, but making no other symmetry assumptions, the average volume expansion rate on the hypersurface of constant proper time of observers comoving with the dust is given by the Buchert equations [67] (see [24, 68, 69] for the case with generalised matter content, including rotation),

$$3\frac{\ddot{a}}{a} = -4\pi G_N \langle \rho \rangle + \mathcal{Q} \quad (2.1)$$

$$3\frac{\dot{a}^2}{a^2} = 8\pi G_N \langle \rho \rangle - \frac{1}{2} \langle {}^{(3)}R \rangle - \frac{1}{2} \mathcal{Q} \quad (2.2)$$

$$0 = \langle \rho \rangle + 3 \langle \theta \rangle, \quad (2.3)$$

where a^3 is proportional to the proper volume, and $H \equiv \frac{1}{3} \langle \theta \rangle = 3\frac{\dot{a}}{a}$ is the average of the local volume expansion rate θ , dot denotes derivative with respect to the proper time of observers comoving with the dust fluid, $\langle \rangle$ is the proper volume average on the hypersurface of constant

proper time and ${}^{(3)}R$ is the spatial curvature. The effect of inhomogeneity and anisotropy is quantified by the backreaction variable \mathcal{Q} ,

$$\mathcal{Q} \equiv \frac{2}{3} (\langle \theta^2 \rangle - \langle \theta \rangle^2) - 2\langle \sigma^2 \rangle , \quad (2.4)$$

where σ^2 is the shear scalar. For a spherical region treated with Newtonian gravity we have $\mathcal{Q} = 0$, as the positive contribution of the variance and the negative contribution of the shear cancel exactly [64]. However, in general, $\mathcal{Q} \neq 0$ for a union of spherical regions, as \mathcal{Q} is not additive. For a homogeneous ellipsoidal region, the variance is zero and the shear is non-zero, so $\mathcal{Q} < 0$ and a homogeneous ellipsoid expands slower than a corresponding sphere with the same density contrast. As in the spherical case, we can have $\mathcal{Q} > 0$ for a union of such regions if the variance of their average expansion rates is larger than the shear contribution.

The density parameters. As in FRW models, the contributions to the expansion rate can be parametrised with relative densities. Dividing (2.1) and (2.2) by $3H^2$, we have [67]

$$q \equiv -\frac{\dot{H}}{H^2} - 1 = \frac{1}{2}\Omega_m + 2\Omega_{\mathcal{Q}} \quad (2.5)$$

$$1 = \Omega_m + \Omega_R + \Omega_{\mathcal{Q}} , \quad (2.6)$$

where q is the deceleration parameter, $\Omega_m \equiv 8\pi G_N \langle \rho \rangle / (3H^2)$, $\Omega_R \equiv -\langle {}^{(3)}R \rangle / (6H^2)$ and $\Omega_{\mathcal{Q}} \equiv -\mathcal{Q} / (6H^2)$ are the density parameters of matter, spatial curvature and the backreaction variable, respectively. It is also useful to define the variance and shear density parameters $\Omega_{\Delta\theta} \equiv -(\langle \theta^2 \rangle - \langle \theta \rangle^2) / (9H^2) = -\Delta\theta / \langle \theta \rangle^2$ and $\Omega_{\sigma} \equiv \langle \sigma^2 \rangle / (3H^2)$, so that $\Omega_{\mathcal{Q}} = \Omega_{\Delta\theta} + \Omega_{\sigma}$. For the sum rules (2.5) and (2.6), it is important that the matter is irrotational dust. This assumption is necessarily violated when collapsing structures stabilise, because turning a collapse around is impossible for irrotational dust. The fact that we consider an ensemble average, not a spatial average, leads to other issues with the density parameters, discussed in section 4.

2.2 Evolution of homogeneous ellipsoids

Dynamical equations. We model structures as homogeneous, non-rotating, anisotropic regions described with Newtonian gravity and embedded in a homogeneous and isotropic background, following [45, 50, 59]. (For a different treatment of ellipsoidal collapse, see [49].) We consider dust matter and a spatially flat background, the evolution of which is described by the Friedmann equations,

$$\begin{aligned} 3\frac{\dot{\bar{a}}^2}{\bar{a}^2} &= 8\pi G_N \bar{\rho} + \Lambda \\ 3\frac{\ddot{\bar{a}}}{\bar{a}} &= -4\pi G_N \bar{\rho} + \Lambda , \end{aligned} \quad (2.7)$$

where $\bar{a}(t)$ is the background scale factor, $\bar{\rho} \propto \bar{a}^{-3}$ is the background density and Λ is the cosmological constant. We also denote $\bar{H} \equiv \dot{\bar{a}}/\bar{a}$.

The gravitational potential Φ in a single region is related to the density by the Poisson equation,

$$\nabla^2 \Phi = 4\pi G_N \rho - \Lambda , \quad (2.8)$$

where the derivatives ∇^2 are with respect to the proper position r^i , and $\rho(t) = \bar{\rho} + \delta\rho$ is the density of the region. The solution of (2.8) that reduces to the background outside the region is¹

$$\Phi = A(t) + B_i(t)r^i + \frac{1}{2}C_{ij}(t)r^i r^j, \quad (2.9)$$

with $\sum_i C_{ii} = 4\pi G_N \bar{\rho} - \Lambda$. As discussed in [50] and mentioned in section 1, this quadratic expression can be understood as a series expansion around an extremum. (Though we will consider extrema of the density, not the gravitational potential.) The spatially constant term is pure gauge, and the linear term corresponds to uniform translation in space, so we set them to zero. The Poisson equation is elliptic, and boundary conditions are needed to fix the non-trace part of the tensor C_{ij} , which describes the deformation. As C_{ij} is symmetric, we can choose coordinates r^i such that C_{ij} is diagonal and write, following the notation of [59],

$$\begin{aligned} \Phi &= \frac{1}{6}(4\pi G_N \bar{\rho} - \Lambda)\delta_{ij}r^i r^j + 2\pi G_N \bar{\rho} \left(\frac{1}{3}\delta + \frac{1}{2}b_i\delta + \lambda_{\text{ext},i} \right) \delta_{ij}r^i r^j \\ &\equiv 2\pi G_N \bar{\rho} C_i \delta_{ij}r^i r^j - \frac{1}{6}\Lambda \delta_{ij}r^i r^j, \end{aligned} \quad (2.10)$$

where the first term on the first line corresponds to the background contribution and on the second line we have defined $C_i(a) \equiv \frac{1}{3}(1 + \delta) + \frac{1}{2}b_i\delta + \lambda_{\text{ext},i}$. Here $\delta \equiv \delta\rho/\bar{\rho}$ is the density contrast with respect to the background, $\frac{1}{2}b_i\delta$ corresponds to tidal effects due to matter inside the region and $\lambda_{\text{ext},i}$ to tidal effects due to matter external to the region. The functions $b_i(t)$ are the eigenvalues of the traceless part (so $\sum_i b_i = 0$) of the internal tidal contribution to C_{ij} ,

$$b_i(t) = a_1 a_2 a_3 \int_0^\infty \frac{dy}{(a_i^2 + y) \prod_{j=1}^3 (a_j^2 + y)^{1/2}} - \frac{2}{3}, \quad (2.11)$$

where $a_i(t)$ are the dimensionless principal axes of the ellipsoid, normalised so that the physical distance is $r^i(t) = a_i(t)x^i$ (no sum), where x^i is the constant coordinate position of a fluid element. The ratio of the proper volume of the region to the background is $a_1 a_2 a_3 / \bar{a}^3$, so $\delta = \bar{a}^3 / (a_1 a_2 a_3) - 1$. Correspondingly, $\lambda_{\text{ext},i}(t)$ are proportional to the eigenvalues of the external part of the tidal tensor, and $\sum_i \lambda_{\text{ext},i} = 0$.

The evolution of a_i is determined by Newton's second law applied to the fluid elements (again, no sum over i),

$$\ddot{r}^i = -\frac{\partial\Phi}{\partial r^i} = -4\pi G_N \bar{\rho} C_i r^i + \frac{1}{3}\Lambda r^i, \quad (2.12)$$

from which we get

$$\ddot{a}_i = -4\pi G_N \bar{\rho} C_i a_i - \frac{1}{3}\Lambda a_i. \quad (2.13)$$

From now on, we put $\Lambda = 0$. It is convenient to rewrite the time derivatives in (2.13) in terms of derivatives with respect to \bar{a} . Using $(\dot{a}/\bar{a})^2 \propto \bar{a}^{-3}$ from (2.7), we obtain

$$a_i'' - \frac{1}{2a}a_i' + \frac{3}{2a^2}C_i(a)a_i = 0, \quad (2.14)$$

¹See [70] for discussion of the meaning of such a potential in Newtonian theory.

where prime denotes derivative with respect to \bar{a} .

In order to solve (2.14), we have to specify the external tides parametrised by $\lambda_{\text{ext},i}(t)$, prescribe how to deal with axes collapsing to zero size, and give the initial conditions. We assume that at early times the region is close to the background, consider only growing modes, and fix the initial conditions at scale factor a_{in} with the Zel'dovich approximation [42],

$$a_i(a_{\text{in}}) = a_{\text{in}}[1 - \lambda_i(a_{\text{in}})] , \quad a'_i(a_{\text{in}}) = 1 - 2\lambda_i(a_{\text{in}}) , \quad (2.15)$$

where λ_i are the eigenvalues of the tidal tensor (i.e. the non-background part of $C_{ij} = \frac{\partial \Phi}{\partial r^i \partial r^j}$) in the linear regime; the normalisation is such that $\sum_i \lambda_i(a_{\text{in}}) = \delta_{\text{in}}$ and the ordering is $\lambda_1 \geq \lambda_2 \geq \lambda_3$. From (2.10) we see that as both b_i and δ are first order small in linear theory, the external tide contribution is required to obtain the correct linear theory result, with $\lambda_{\text{ext},i}(a) = \frac{a}{a_{\text{in}}}[\lambda_i(a_{\text{in}}) - \frac{1}{3}\delta_{\text{in}}]$ in the linear regime. Unlike in the spherical case, the environment cannot be neglected if the ellipsoid is embedded in an FRW universe; dropping external tides would correspond to the case of an isolated ellipsoid considered in [45]. We will consider non-linear evolution, so we need to make further assumptions to define $\lambda_{\text{ext},i}$ outside of the linear regime.

Non-linear external tides. Different prescriptions have been proposed for non-linear external tides. In [47] they were calculated approximately from a series of spherical shells, neglecting angular distribution of matter within each shell. In [50] the following linear and non-linear models were proposed:

$$\lambda_{\text{ext},i}(a) = \frac{a}{a_{\text{in}}} \left[\lambda_i(a_{\text{in}}) - \frac{1}{3}\delta(a_{\text{in}}) \right] \quad \text{linear} \quad (2.16)$$

$$\lambda_{\text{ext},i}(a) = \frac{5}{4}b_i(a) \quad \text{non-linear} . \quad (2.17)$$

The linear prescription simply extrapolates the functional form of the linear case into the non-linear regime, whereas the non-linear prescription is a simple ansatz that has the same linear behaviour, but is dominated by internal dynamics in the non-linear regime. In [59], the two forms were mixed into the hybrid model, where external tide $\lambda_{\text{ext},i}$ follows the non-linear model (2.17) in the direction i , unless the axis i turns around, i.e. $\dot{a}_i = 0$, in which case the evolution follows the linear model (2.16) after turnaround.

The linear model is unsuitable for our purposes, because we consider underdense as well as overdense regions. If an underdense region does not collapse, its density evolution at late stages is much slower than the extrapolation of the linear regime behaviour (because the density contrast cannot become more negative than -1), and the linear tide would dominate and give unphysical results. We have considered both the non-linear and the hybrid model. For our case, the difference is negligible, and we show results only for the non-linear model.

Virialisation. If an ellipsoid starts to collapse along an axis, the axis will shrink to zero in a finite time, leading to infinite density. As the matter is irrotational dust, there is nothing to stop the collapse, so a prescription for virialisation has to be added. In the spherical case considered in [33] this did not make much difference, because when all directions collapse at the same time, the proper volume of the structure is small at collapse, and it has negligible effect on the average, as the volume goes to zero faster than the expansion rate diverges. However, when only one direction collapses, the volume of the structure is not necessarily

negligible, and indeed filaments and walls occupy a sizeable fraction of the volume of the real universe [40, 41].

We adopt the prescription based on the tensor virial theorem used in [59]. At the instant when the virialisation condition is satisfied for axis i , the collapse is stopped and a_i is frozen at the value it has at that point. This means that the acceleration in direction i is momentarily divergent, and energy is not conserved. As we average the expansion rate, not the acceleration, this does not make a difference.

Initial conditions. We have now fully defined the dynamical equations for the axis lengths a_i . Next we should specify the initial conditions, which in the Zel'dovich approximation reduce to the distribution of $\lambda_i(a_{\text{in}})$; in what follows, we drop the subscript “in” when referring to the initial values of λ_i and δ . Our regions are a model for nonlinear structure, which we take to form on extrema (peaks and troughs) of the density field, taken to be Gaussian, as expected from inflation and confirmed by observations [71]. We parametrise the initial conditions in terms of the peak height (or trough depth) given by the density contrast $\delta = \sum_i \lambda_i$, and the shape given in terms of the ellipticity e and prolateness p , defined as

$$e = \frac{\lambda_1 - \lambda_2}{2\delta} \ , \quad p = \frac{\lambda_1 - 2\lambda_2 + \lambda_3}{2\delta} \ . \quad (2.18)$$

We would like to have the distribution of δ , e and p , on the condition that we are at an extremum of the density field. For δ , the probability distribution conditioned on the existence of an extremum was calculated in [72]. The unconditional distribution of e and p was worked out in [42, 73], and the conditional joint distribution for e and p , given δ (and assuming $\delta > 0$), is given in [53] (equation A3). However, finding the distribution of e and p under the additional condition that the density field has an extremum is not straightforward. Note that λ_i are the eigenvalues of the tidal tensor, and they determine whether the gravitational potential Φ has an extremum, and this does not necessarily coincide with an extremum of the density contrast δ . The tidal matrix and the matrix given by the Hessian of δ do not commute, so they cannot be diagonalised simultaneously, and finding the distribution of the eigenvalues of the former under a condition for the eigenvalues of latter is a non-trivial problem [74]. For the number density of peaks/troughs we use the result of [74] (equation 37). It requires as input the values of e and p . For the distribution of e and p we use the result of [53], modified to take into account that we can have $\delta < 0$. This distribution has been conditioned on the value of δ , but not on the requirement that there is a peak/trough. This is not expected to make a large difference (see e.g. figure 3 of [74]), because regions with large density contrast often contain extrema, and regions with small density contrast don't have a large effect. As the overall impact of deviations from spherical symmetry turns out in our case to be small, conditioning the distribution of e and p on the existence of an extremum would be a small correction to a small effect.

2.3 The average expansion rate

Ensemble of ellipsoids. We consider a model where the volume of the universe is divided into peaks/troughs, which evolve according to the ellipsoidal model discussed above, and smooth regions, which evolve like the background. As the peaks/troughs expand and collapse and their volume fractions of change, the average expansion rate evolves. We calculate the average expansion rate as follows, generalising the spherical expression in [33] to include

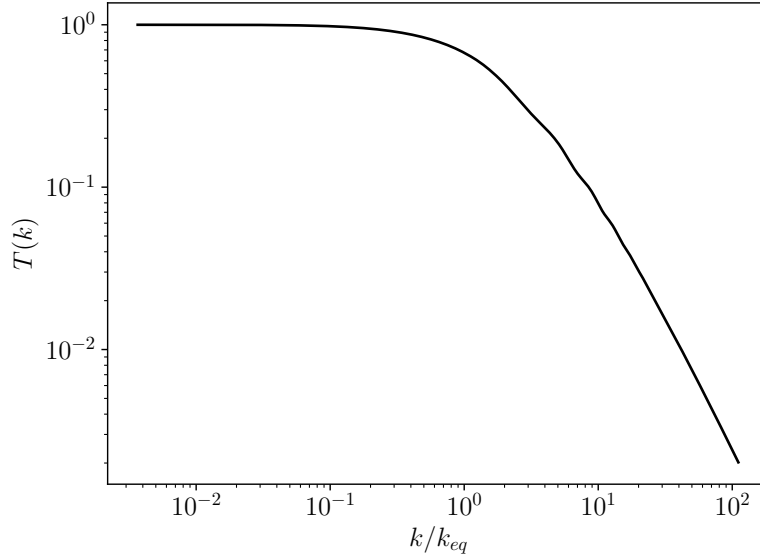


Figure 1: Transfer function of a cold dark matter (CDM) model with $\omega_b = 0.02$ and $\omega_m = 0.14$ and no dark energy, calculated with CAMB [75]. Wavenumbers are in units of the matter-radiation equality scale k_{eq} .

ellipticity and prolateness:

$$\begin{aligned}
 H(t) &= \int d\delta de dp v(\delta, e, p, t) H(\delta, e, p, t) \\
 &= \frac{\int d\delta de dp f(\delta, e, p, t) s(\delta, e, p, t) H(\delta, e, p, t)}{\int d\delta de dp f(\delta, e, p, t) s(\delta, e, p, t)}, \quad (2.19)
 \end{aligned}$$

where $v(\delta, e, p, t)$ is the fraction of volume, at time t , in regions that had initial linear density contrast δ , ellipticity e and prolateness p , and $H(\delta, e, p, t) = \frac{1}{3} \sum_i \frac{\dot{a}_i}{a_i}$ is the expansion rate, at time t , of a region with such initial conditions. The volume fraction $v = sf / [\int d\delta de dp sf]$ has two parts. The factor $s(\delta, e, p, t) \equiv a_1 a_2 a_3 / \bar{a}^3$ is the volume of a region with initial linear density contrast δ , ellipticity e and prolateness p , relative to the background volume, at time t . It depends only on how the region expands relative to the background. The factor $f(\delta, e, p, t)$ is the number density of extrema with initial δ, e and p , at time t . It depends on how the number density of peaks and troughs changes with time. The peak number density is defined for a given smoothing scale R and thus depends on the choice of R ; we use a Gaussian window function. We take the primordial power spectrum to be a power law with spectral index $n = 0.96$ (at the pivot scale $k = 0.05 \text{ Mpc}^{-1}$) [71]. We take the transfer function of a cold dark matter (CDM) model with $\omega_b = 0.02$ and $\omega_m = 0.14$ and no dark energy, calculated with CAMB² [75] and plotted in figure 1. These values, usually determined in the Λ CDM FRW model [71], are model-independent [76].

As in [33], we fix the smoothing scale $R(t)$ by demanding that the root mean square density contrast is unity at all times, $\sigma_0[R(t), t] = 1$. The timescale of changes is thus determined by location of the turnover in the transfer function, which comes from the matter-

²<http://camb.info>

radiation equality time $t_{\text{eq}} = 5 \times 10^4$ yr. The idea is that R determined like this gives the scale for typical structures. The precise numbers of our results depend on the choice of value for $\sigma_0(R, t)$, as we will see in section 3, but as in [33], the qualitative behaviour and the order of magnitude are the same as long as $\sigma_0(R, t)$ is of order unity. As density perturbations evolve in time, R grows to compensate, modelling the merging of structures into larger ones. Volume that is neither in peaks nor troughs is taken to evolve like the background. We fix the normalisation of the number density by demanding that in the asymptotic future all volume will be in peaks or troughs.

In the same way, the average shear scalar is calculated as

$$\langle \sigma^2 \rangle = \frac{1}{3} \int d\delta d\epsilon d\epsilon d p v(\delta, \epsilon, p, t) \left(\sum_i \frac{\dot{a}_i^2}{a_i^2} - \sum_{i < j} \frac{\dot{a}_i \dot{a}_j}{a_i a_j} \right). \quad (2.20)$$

3 Results

3.1 The average expansion rate

We calculate the averages (2.19) and (2.20) numerically. The functions a_i are calculated from (2.14) with the initial conditions (2.15), using the initial distributions for λ_i discussed in section 2.2, with the virialisation condition based on the tensor virial theorem given in [59], and the non-linear prescription for the external tides. For comparison, we present the results for the case when the peaks are spherical, calculated with the same primordial power spectrum and transfer function.

In figure 2 we show the expansion rate Ht as a function of $k_{\text{eq}}R$ (k_{eq} is the comoving wavenumber of the modes that cross the Hubble radius at matter-radiation equality) and t . At early times, the expansion rate is close to the background Einstein–de Sitter case $Ht = 2/3$ (we do not consider radiation, so the model does not apply at times earlier than $\sim 10^6$ years). As the underdense regions that expand faster than the background take up more of the volume, Ht rises, with a transition at $R \sim k_{\text{eq}}^{-1}$, corresponding to $t \approx 10^7 t_{\text{eq}} \approx 10^3$ Gyr. The value practically saturates at $Ht = 0.83$ at very late times $t \approx 10^5$ Gyr. (Note that the age at late times is exponentially sensitive to the value of R .)

Because the ellipsoids are homogeneous, the expansion is slower than in the spherical case, as discussed in section 2.1. Therefore the expansion rate in the ellipsoidal case is always smaller than in the spherical case, where the asymptotic value is $Ht = 0.85$. (An ellipsoid can expand faster than a spherical region in the sense that it may continue expanding in one or two directions after a sphere has already collapsed, but the effect of such regions on the average is small.) The fact that every individual region expands slower does not necessarily mean that the average expansion rate is smaller, nor that the corresponding acceleration is smaller, because \mathcal{Q} is not additive. In fact, having some regions slow down more can lead to acceleration [22, 66, 77, 78]. Nevertheless, in our case the shear is too small and its rise is not rapid enough to give acceleration.

The deceleration parameter q is plotted in figure 3. The blue line is obtained using the first equality in (2.5), $q = -\dot{H}/H^2 - 1$. We always have $q > 0$, so the expansion decelerates; at late times, the expansion rate asymptotes to $Ht = 0.83$, which corresponds to $q = 0.2$. We can then determine Ω_{m} by the second equality in (2.5) as $\Omega_{\text{m}} = 2q - 4\Omega_{\mathcal{Q}}$, and the spatial curvature density parameter from (2.6) as $\Omega_R = 1 - \Omega_{\mathcal{Q}} - \Omega_{\text{m}}$. The resulting density parameters are plotted in figure 4 (solid lines). The universe transitions around $R \sim k_{\text{eq}}$

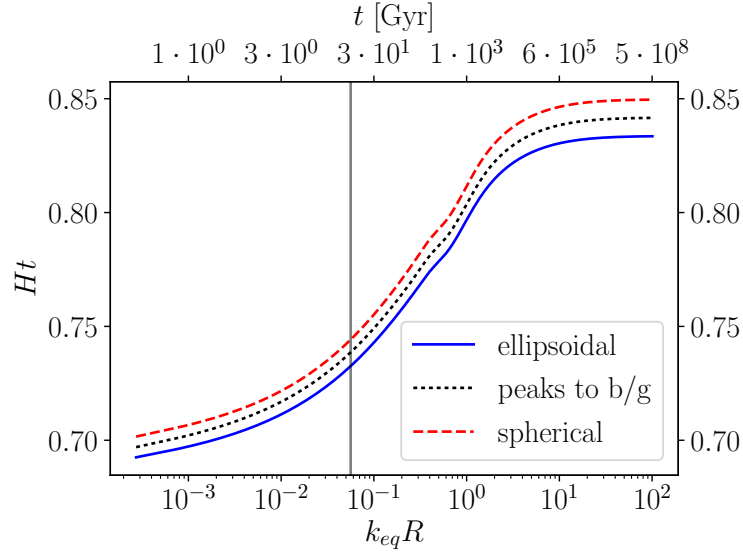


Figure 2: The expansion rate times the age of the universe, Ht , for the full ellipsoidal case (solid blue), spherical case (red dashed) and the ellipsoidal case when peak volume is assigned to the background (black dotted). The axis at the top shows the age of the universe corresponding to the $k_{eq}R$ value on the bottom axis. The vertical line corresponds to $t = 14$ Gyr.

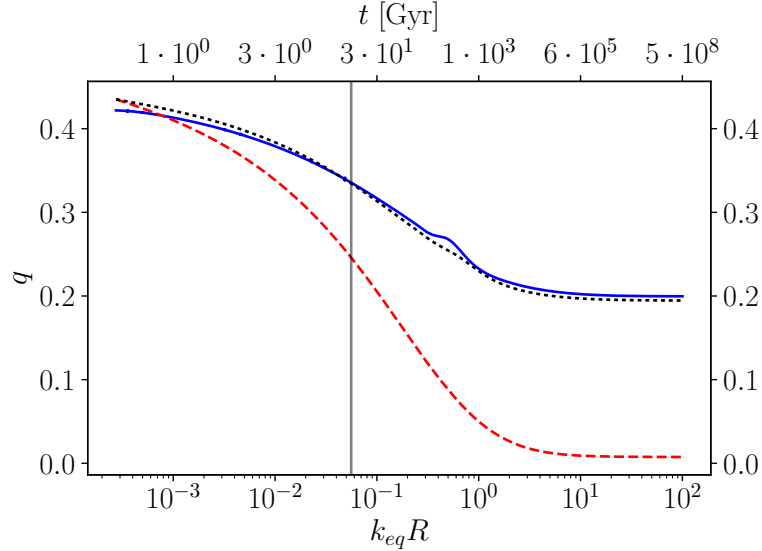


Figure 3: The deceleration parameter q determined by calculating Ht from the ensemble and using (2.5) (blue), calculating Ht and the proper volume from the ensemble to give Ω_m and using (2.5) (black dotted) or calculating Ht from the ensemble and finding Ω_m from Ht (red dashed). See section 4 for details.

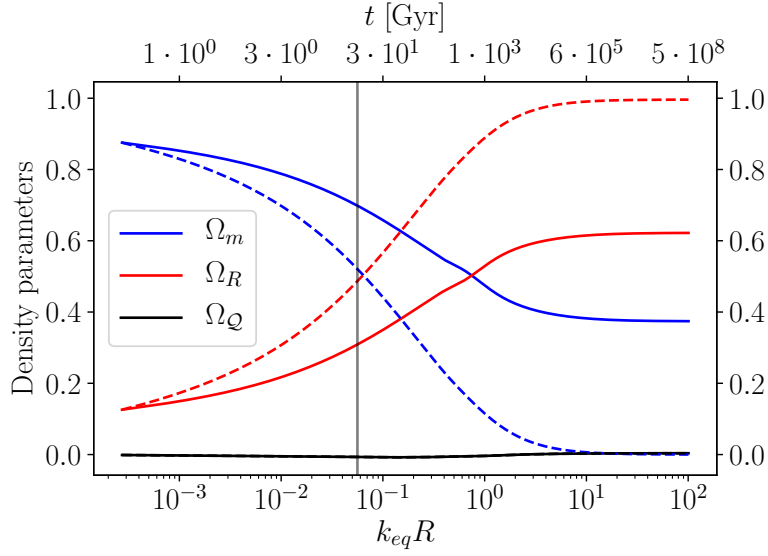


Figure 4: The density parameters Ω_m (blue), Ω_R (red) and Ω_Q (black). Solid lines correspond to Ω_m determined using (2.5), dashed lines to the case when Ω_m is calculated from Ht . See section 4 for details.

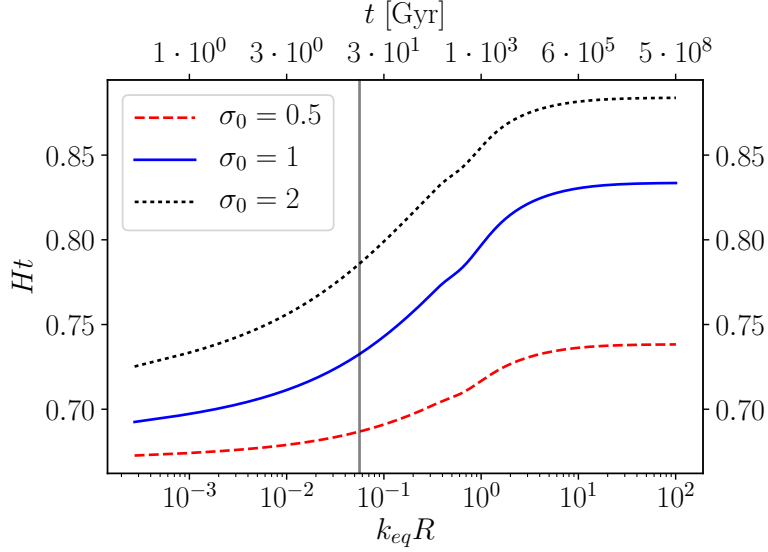


Figure 5: The expansion rate Ht for $\sigma_0(R, t)$ equal to 0.5 (red, bottom), 1 (blue, middle) and 2 (black, top). Note that the top t values correspond to the case $\sigma_0(R, t) = 1$. For the other cases they are larger or smaller by a factor of $2^{3/2} \approx 3$.

from being close to matter-dominated to the asymptotic values $\Omega_m = 0.37$, $\Omega_R = 0.62$. The backreaction variable remains small throughout, $|\Omega_Q| < 0.01$.

The precise numbers depend on how the smoothing scale has been set. In figure 5 we

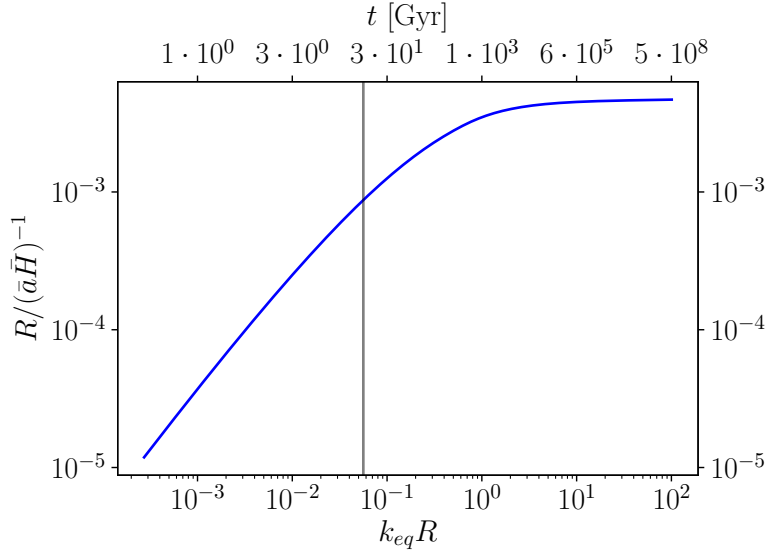


Figure 6: The smoothing scale, corresponding to the typical size of structures, relative to the background Hubble length, $R/(\bar{a}\bar{H})^{-1}$.

show Ht in the cases when $\sigma_0(R, t)$ is chosen to be 0.5, 1 or 2. A factor of 2 variation in the linear density contrast around unity typically corresponds to a large change in the non-linear evolution; in the spherical model, regions with linear density contrast of 2 have already completely collapsed. We see that the magnitude of the change in Ht relative to the Einstein-de Sitter value $2/3$ goes from 11% to 25% and 32% for the cases $\sigma_0(R, t) = 0.5$, 1 and 2, respectively. However, the qualitative behaviour and the order of magnitude of the change and its timing stay the same.

The transition era $R \sim k_{\text{eq}}^{-1}$ is also visible in figure 6, where we compare the smoothing scale $R(t)$ (indicative of the size of largest structures at time t) to the comoving background Hubble length $(\bar{a}\bar{H})^{-1}$. Structures start small, their relative size grows rapidly and continues to grow slowly after the transition. The reason is that for $k < k_{\text{eq}}$, the transfer function is essentially constant. If the primordial spectrum were scale-invariant, then there would be no scale in the system any more, and dimensionless quantities like $R/(\bar{a}\bar{H})^{-1}$ would be constant. With a non-scale-invariant spectrum, $n = 0.96$, there is still slow evolution.

3.2 The shear

In figure 7 we show the fraction of volume in the peaks, troughs and the background. The results are almost the same in ellipsoidal and spherical cases. Between $k_{\text{eq}}R = 0.1$ and $k_{\text{eq}}R = 1$ (corresponding to $t = 30$ Gyr and $t = 10^3$ Gyr, respectively) troughs start to dominate the volume. This happens both because their fraction of initial volume (which is also the mass fraction) grows due to merging and because they expand faster than the background. In figure 8 we show the mass fraction of regions that have collapsed along one, two or three axes, corresponding to walls, filaments and clusters. The transition is clear also here, and the fractions practically saturate around $R = k_{\text{eq}}^{-1}$. (After the transition, the volume fraction of all these regions is negligible, as figure 7 shows.) Unlike the spherical model, the ellipsoidal case allows underdense regions to collapse due to decelerating effect

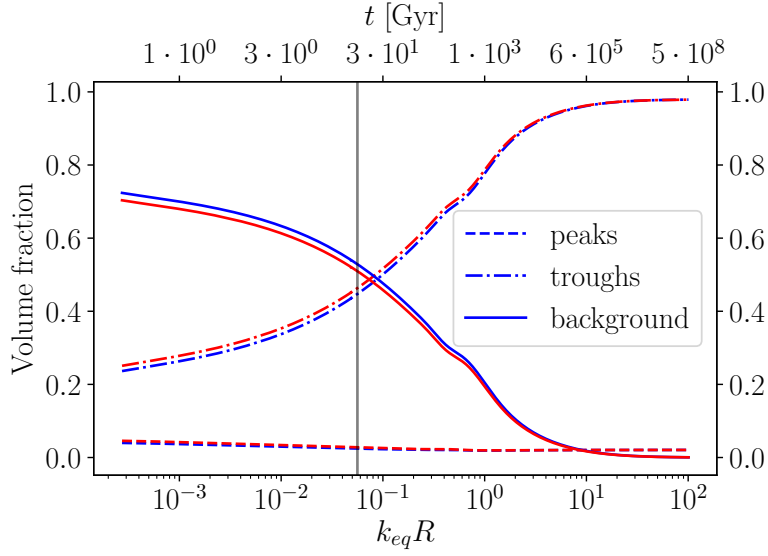


Figure 7: The fraction of volume in peaks (dashed), in troughs (dot-dashed) and in the background (solid). The blue line is the ellipsoidal case and the red line is the spherical case.

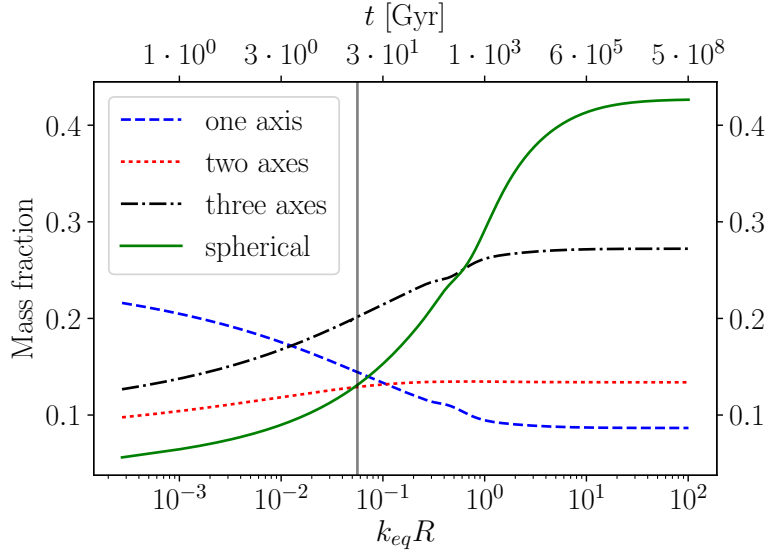


Figure 8: The fraction of regions that have collapsed along 1, 2 or 3 axes (not weighted by volume). The spherical case is shown for comparison.

of shear, but the troughs are so deep that this has negligible effect on the averages. The mass fraction of structures that have collapsed at least on one axis peaks at 49%. After the transition, 27% of the mass is in clusters, 14% in filaments and 8% in walls. Compared to simulations and observations of structure, our model is missing efficient flow of mass from underdense to overdense regions [40, 41].

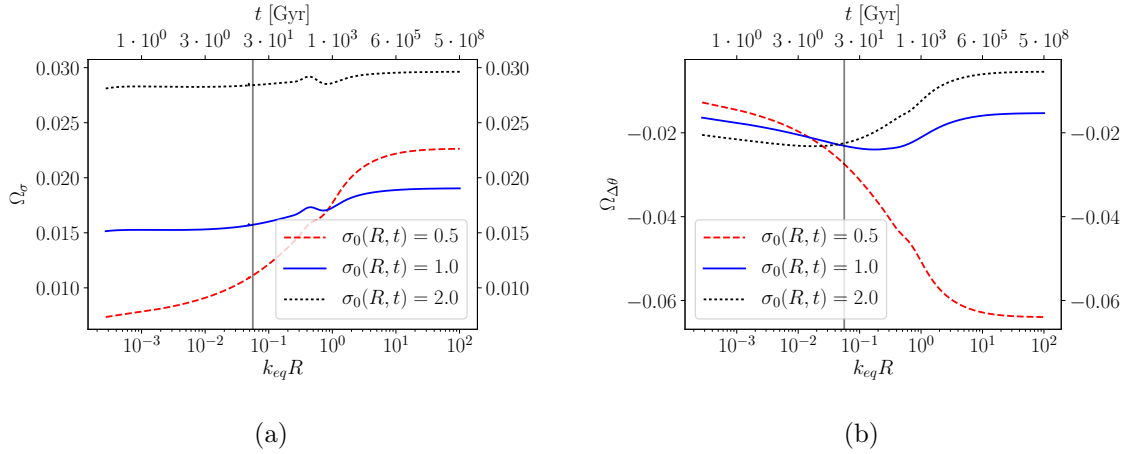


Figure 9: The shear density parameter Ω_σ (left) and the variance density parameter $\Omega_{\Delta\theta}$ (right) for $\sigma_0(R, t)$ equal to 0.5 (red), 1 (blue) and 2 (black).

Figure 9a shows the effect of the shear in terms of Ω_σ for different choices of $\sigma_0(R, t)$. For $\sigma_0(R, t) = 1$, the amplitude is between 1% and 2%, an order of magnitude below what would be required to have a significant impact on the average expansion rate. In this case, unlike for the other quantities, the difference between the non-linear and hybrid treatments would be discernible by eye in the plots, but the absolute difference is only at the level 0.003. The variation due to changing the value of $\sigma_0(R, t)$ is much larger than this. If we set $\sigma_0(R, t) = 2$, we keep more non-linear regions, resulting in larger shear. For $\sigma_0(R, t) = 0.5$, there are fewer non-linear regions and the shear is initially smaller, but grows slightly larger at late times. These variations do not change the order of magnitude of the shear contribution, which remains below 3%.

The evolution of the variance is shown in figure 9b. For $\sigma_0(R, t) = 1$, at early times the variance is small because most of the volume evolves like the background, and at late times the variance is small because the volume is dominated by underdense regions with expansion rates close to each other (though far from the background). The transition era with peak variance is a bit before $R = k_{eq}^{-1}$. In the ellipsoidal case the variance is smaller than in the spherical case by a factor of 1.5, as shown in figure 10, because the shear decelerates the expansion more, so troughs remain closer to the background. As in the case of the shear, changing the value $\sigma_0(R, t)$ affects the qualitative evolution of $\Omega_{\Delta\theta}$, but not the order of magnitude, the maximum amplitude remaining smaller than 7% in all cases.

In figure 11a, we show the shear density parameter Ω_σ for the troughs only, compared to the full result. The shear of troughs goes down with time, because they become more spherical as they expand. In contrast, the shear of peaks rises as the axes become more differentiated. The shear has a bump around k_{eq} , where the peak number density grows rapidly, and peak contribution rises, followed by a dip as the trough contribution falls. Figure 11b shows $\Omega_{\Delta\theta}$ for the troughs and for the full result. Complementing the shear plot, it shows that the variance of the troughs goes down with time, but the overall variance amplitude has a bump around k_{eq} due to peaks becoming more differentiated, and their contribution to the average then goes down due to their shrinking volume.

Figure 12a shows that the shear density parameter for the peaks alone grows large around $k = k_{eq}$, to $\Omega_\sigma = 1.5$. The evolution of the variance, shown in figure 12b, matches

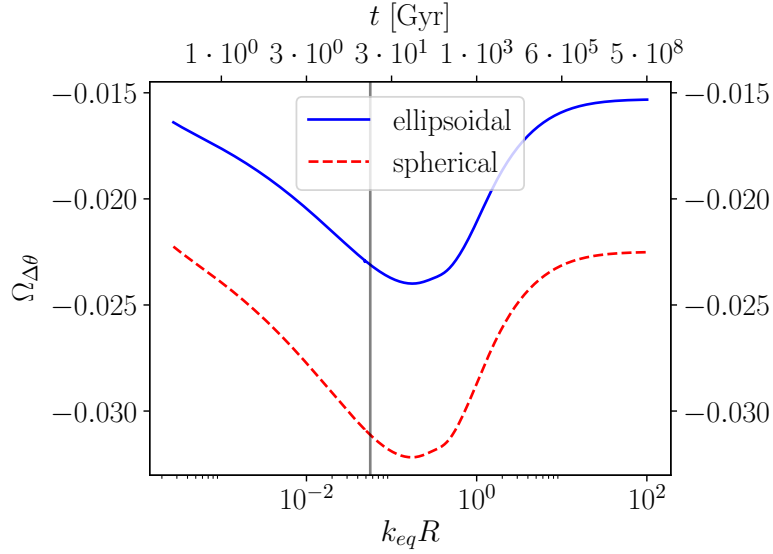


Figure 10: Comparison of the variance density parameter $\Omega_{\Delta\theta}$ for the spherical (red, lower) and ellipsoidal (blue, upper) cases.

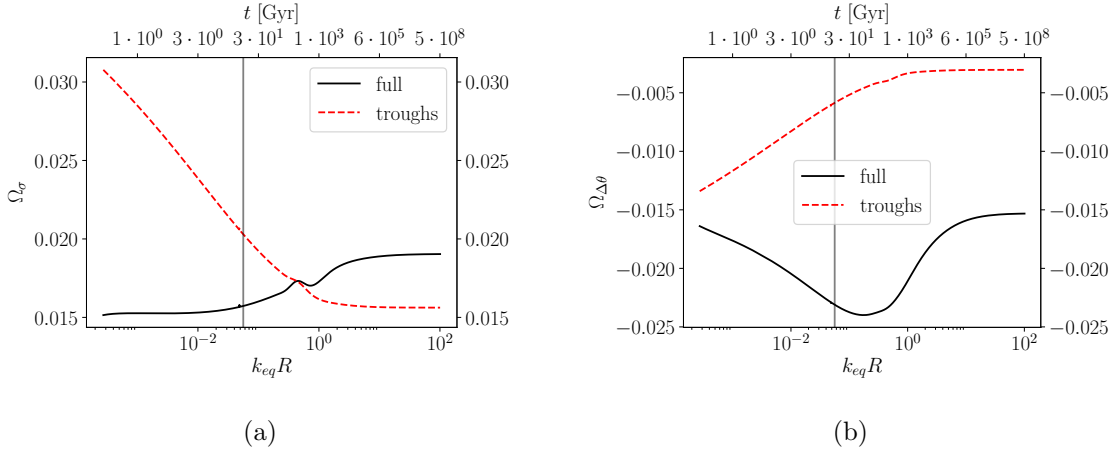


Figure 11: The shear density parameter Ω_σ (left) and the variance density parameter $\Omega_{\Delta\theta}$ (right) for the full result (black) and the troughs alone (red).

that of the shear, with $\Omega_{\Delta\theta}$ reaching the value -1.2 for the peaks. However, as the volume fraction of peaks simultaneously falls, their impact on the average expansion rate becomes smaller. In figure 13 we show Ht for the peaks, troughs and the full sample of regions, which shows how the peaks bring down the expansion rate. In figure 2 the solid black line shows what happens if we allocate the volume of the peaks for the background (i.e. their volume factor is as small as in the usual case, but they expand like the background). This shows that the growth of Ht can mostly be understood simply in terms of the faster-expanding troughs taking up more a larger fraction of space, but there is also a small contribution from the peaks, bringing Ht down.

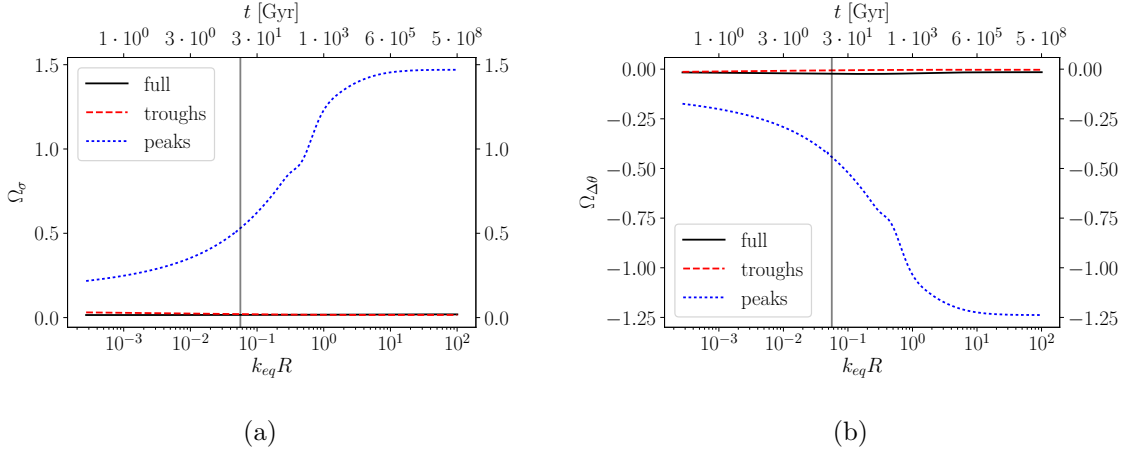


Figure 12: The shear density parameter Ω_σ (left) and the variance density parameter $\Omega_{\Delta\theta}$ (right) for the full result (black), troughs (red) and peaks (blue).

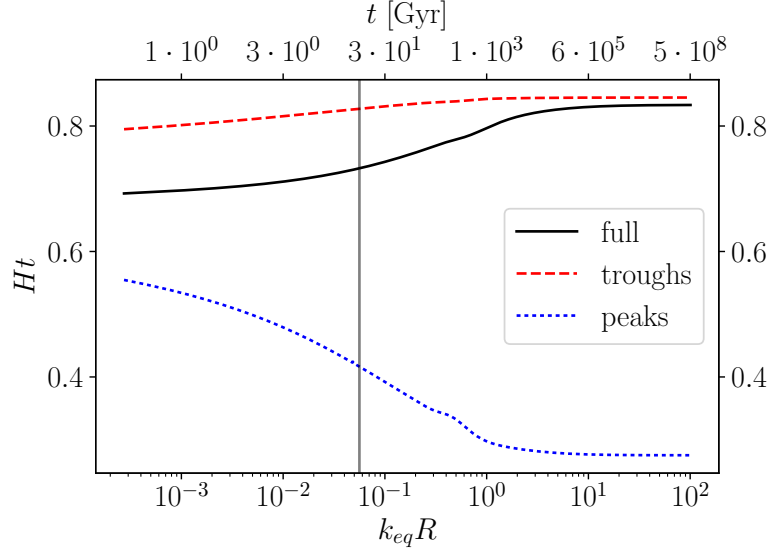


Figure 13: The expansion rate Ht for the full result (black), troughs (red) and peaks (blue).

The variance and shear contribute with the opposite sign to \mathcal{Q} , so their contributions cancel to make $\Omega_{\mathcal{Q}}$, shown in figure 14, smaller than either Ω_σ or $|\Omega_{\Delta\theta}|$ and negative, with an extremum amplitude of $\Omega_{\mathcal{Q}} = -0.008$ reached at $0.1k_{\text{eq}}$. Such a close cancellation is not a robust result: as figure 9 shows, for $\sigma_0 = 0.5$ the extremum value is $\Omega_{\mathcal{Q}} = -0.04$ and for $\sigma_0 = 2$ it is $\Omega_{\mathcal{Q}} = 0.024$. In the spherical case the variance and shear of each region cancel individually, and in the average over regions only the variance term appears, with an extremum of $\Omega_{\mathcal{Q}} = -0.03$. According to (2.5), the observed values $q \approx -0.5$ and $\Omega_m \approx 0.3$ correspond to $\Omega_{\mathcal{Q}} \approx -0.3$, an order of magnitude above the largest numbers here.³

³The value $q \approx -0.5$ is the Λ CDM model result. The value depends on the chosen parametrisation [79, 80]. The value has also been derived under the assumption that light propagation is related to the expansion rate

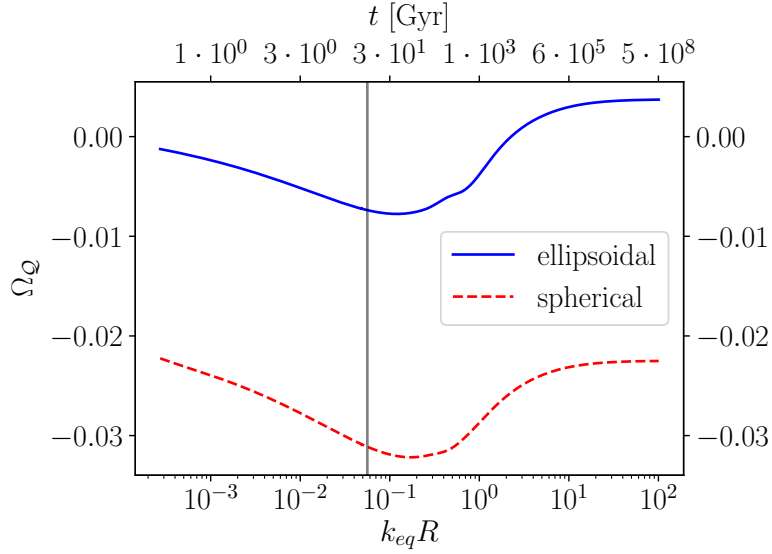


Figure 14: The backreaction density parameter Ω_Q for the ellipsoidal (blue) and spherical (red) case.

4 Discussion

Successes and shortcomings. Structures have a large impact on the expansion rate, and Ht grows by 25% relative to the Einstein–de Sitter value $2/3$. This change of the same order of magnitude, but slightly smaller, than in the spherical case. The matter density parameter Ω_m correspondingly falls by a factor of about 3 from 1 to 0.37. These are asymptotic values, reached at $R = 9k_{eq}^{-1}$ (corresponding to $t \sim 10^5$ Gyr). The order of magnitude of the change from the Einstein–de Sitter case corresponds to present-day observations.⁴ Combining the measurement $H_0 = 72.5 \pm 3.2$ km/s/Mpc [83] (for other determinations of H_0 , see [84]) with a model-independent determination of t_0 [85] gives $H_0 t_0 = 0.99 \pm 0.04$ for the central value $t_0 = 13.4$ Gyr, and $H_0 t_0 > 0.83$ for the central value of H_0 and the lower limit $t_0 > 11.2$ Gyr. Both of these agreements were noted in [33] for the spherical collapse model.

The orders of magnitude are easy to understand. The Einstein–de Sitter universe has $Ht = 2/3$ and a universe without matter and dominated by spatial curvature has $Ht = 1$. Therefore, if the volume is dominated by voids but not completely empty, $2/3 < Ht < 1$. The timing comes from the fact that the transfer function rises when approaching k_{eq} from above, so when modes with smaller wavenumber form non-linear structures, the number density of troughs grows, as shown in figure 7. After modes with $k \sim k_{eq}$ collapse, the transfer function is practically constant, as shown in figure 1. As the change in the transfer function is not sharp and peaks have only a small impact, the change in Ht is not sharp.

Indeed, the matter-equality scale is the only scale that has a large impact on structure

via the FRW distance-redshift relation, which is not necessarily the case if backreaction is large [17, 22–26].

⁴Note that the large value of the spatial curvature parameter $\Omega_R = 0.62$ is not in obvious contradiction with observations, as tight limits on spatial curvature [71, 81, 82] only apply if it evolves like $\langle {}^{(3)}R \rangle \propto (1+z)^2$, and in this case $\langle {}^{(3)}R \rangle$ falls more rapidly to the past, and therefore has a smaller effect on the angular diameter distance [22].

formation, apart from the free-streaming cut-off at large wavenumbers, which determines the beginning of structure formation [86] (the baryon acoustic oscillation scale, for example, is only a small correction). The time when modes with wavenumber k_{eq} form structures is related to the matter-radiation equality time $t_{\text{eq}} = 5 \times 10^4$ yr roughly as $t \sim A^{-3/2} t_{\text{eq}} \sim 10^2$ Gyr, where $A = 5 \times 10^{-5}$ [71] is the primordial amplitude of perturbations [33]. With the relation between t and R given by $\sigma_0(R, t) = 1$, the age at late times is exponentially sensitive to the value of R , so we should avoid reading too much into the feature that the large values roughly corresponding to present-day observations are reached for times that are a few orders of magnitude larger than the than observed timing of the acceleration in the real universe. The fact that the relevant timescale for the start of significant backreaction is billions of years is robust. There is thus no coincidence problem, and anthropic arguments for the acceleration timescale related to the existence of highly evolved bound structures needed to produce observers like us are reduced to the change in the expansion rate coinciding with a late period in structure formation.

The details of the expansion history are different from the observations. This may not be too worrisome, given the simplicity of the model, which is missing many physical effects. Our treatment of structure formation is rather simplistic, as shown by the fact that half of the mass remains in underdense regions. The feature that smaller peaks may reside inside larger peaks and that troughs can be extinguished by peaks, known as the cloud-in-a-cloud and the void-in-a-cloud problem, respectively, is not included; for discussion in the context of the peaks formalism, see [61, 62]. Taking this into account would transfer mass from underdense to overdense regions. Another problem is that peaks and troughs are assumed to contain the same mass regardless of depth. Also, the merging together of structures is dealt with only via the Gaussian smoothing, and the constraint $\sigma_0(R, t) = 1$ is rather approximate. The condition that all matter is in troughs and peaks at late times is somewhat arbitrary, and only strictly works if the spectrum is scale-invariant; for a red spectrum, the peak number density keeps rising. The treatment of the individual regions as either anisotropic but homogeneous (in the ellipsoidal model) or inhomogeneous but isotropic (in the spherical model) could also be improved. One possibility would be to use an exact general relativistic model, such as the Szekeres model [87], the most general known dust solution. However, if holes are removed from a FRW universe and filled with a regular Szekeres dust model, backreaction is small if the holes are small compared to the Hubble scale and the matching between the hole and the background is taken into account [17]. But the description of matter as dust breaks down due to shell crossings in the course of structure formation, and rotation also becomes non-negligible [88]. Also, the Szekeres model is limited in the sense that the magnetic part of the Weyl tensor is zero, so there is no exchange of information between worldlines comoving with the dust; it is conjectured that generalisation of the model would violate this [89]. Vanishing magnetic part of the Weyl tensor is a property shared by Newtonian gravity, whereas it is important for real structure formation [37, 90]. In the Newtonian limit, the magnetic part of the Weyl tensor is related to spatial curvature [91] (see also [28]).

Apart from issues with modelling the individual regions, the ensemble treatment has consistency problems. We have calculated the expansion rate H , the variance $\Delta\theta$ and the shear $\langle\sigma^2\rangle$ from the ensemble. We have then determined Ω_Q from its definition using these quantities. The quantities q and Ω_m have been calculated from the Buchert equations with H , using the first and second equality of (2.5). We would get roughly the same answer if we were to use the definition $\Omega_m \propto \langle\rho\rangle/H^2$, taking $\langle\rho\rangle$ to be inversely proportional to the volume calculated from the ensemble average used as the volume factor in (2.19) and then

using the second equality of (2.5). The resulting q is shown in figure 3 in black.⁵

The problem is that this volume does not agree with the volume calculated from the expansion given by H , which is $\propto e^{3\int dt H(t)}$. As the expansion rate is faster than in the Einstein–de Sitter case, the corresponding Ω_m decreases without limit. The deceleration parameter q and the density parameters determined by calculating Ω_m (instead of q) from the expansion rate Ht are shown in figures 3 (black line) and 4. This is physically reasonable: when the volume becomes dominated by very empty regions, the variance and shear become small, so the evolution should tend to the FRW universe dominated by negative spatial curvature, with Ω_m approaching zero. Backreaction can interpolate between two FRW cases, but it cannot continue to be important when the universe becomes smooth. (Non-negligible residual variance and shear could asymptotically persist due to ongoing structure formation, so that the evolution does not asymptotically approach $Ht = 1$, but Ω_m would nevertheless approach zero if the expansion is faster than in the Einstein–de Sitter case.)

The form of the Buchert equations (2.1)–(2.3) and the resulting density parameter relations (2.5) and (2.6) that we have used rely on the matter evolving like irrotational dust. Virialisation and our treatment of the merging of structures violate this assumption, so there are terms missing from the equations. However, the above inconsistency cannot be laid at the door of the dust assumption. The root of the problem is that we consider an ensemble of regions with different expansion rates, not an ensemble of regions with different volumes. More precisely, the expansion rate we consider involves the time derivative of the factor s in (2.19) that accounts for the growth factor for individual regions, but not f , which models the merging together of regions. Simply put, if Ht is constant and $> 2/3$, then Ω_m cannot be a non-zero constant, so calculating them both directly using the ensemble quantities that practically saturate after $k_{\text{eq}}R \approx 9$ (or equivalently $t \approx 4 \times 10^5$ Gyr) is not consistent.

A related issue is that the structures evolve in the background space, unaffected by the deviation of the expansion rate from the background. A small aspect of this is that when the expansion becomes faster, the growth of density perturbations should change. A potentially more important factor is that the volume factor in the ensemble average (2.19) for regions that have stopped evolving, i.e. ones corresponding to $k^{-1} \ll R$, is equal to the background volume. However, even if the structures on small scales have stopped evolving, their volume should reflect the extra expansion that has taken place relative to the background. Correcting the volume factor should also take into account the discrepancy between the ensemble volume and the volume determined from the expansion rate. However, the usefulness of such improvements is conditional on making sure that the distinction between Newtonian and relativistic behaviour is correctly implemented in the statistical treatment.

Newtonian and relativistic treatment. Our calculation looks completely Newtonian. However, in the Newtonian case the contribution of the variance and the shear to \mathcal{Q} cancel each other up to a boundary term [14]. For a statistically homogeneous and isotropic distribution, the boundary term is small, so the expansion rate is close to the FRW value, whereas we have found significant differences. It was noted in [33] that the resolution is that in the Newtonian case total energy is conserved, and we have not implemented such a global constraint on the peak statistics. In contrast, in the relativistic case the total energy is not a well-defined quantity. The corresponding term in the equations for the average expansion

⁵In [33], the analogue between a spherical Newtonian model and the relativistic dust FRW model was used to calculate Ω_R , and the matter density parameter was then determined as $\Omega_m = 1 - \Omega_R - \Omega_Q$. This gives equivalent results in the spherical case, but there is no such simple analogue in the ellipsoidal case.

rate is the spatial curvature, for which there is no conservation law: there is no requirement for the positive spatial curvature of overdense regions to exactly balance the negative spatial curvature of underdense regions in the course of evolution [9, 92]. It was therefore argued in [33] that a calculation like the one presented here is closer to the relativistic situation: even if the individual regions are Newtonian, their distribution does not follow the Newtonian pattern. Of course, in a full and consistent calculation, the distribution of regions should flow from the process of regions joining together, which in our calculation is modelled only by changing the smoothing scale.

Let us consider the energy argument more carefully. In Newtonian theory, the total energy of a distribution of self-gravitating dust is (see e.g. [50])⁶

$$\begin{aligned} E &= \frac{1}{2} \sum_i m_i \dot{\bar{x}}_i^2 - G_N \sum_{i < j} \frac{m_i m_j}{|\bar{x}_i - \bar{x}_j|} \\ &= \frac{1}{2} \int d^3x \rho(t, \bar{x}) \bar{v}(t, \bar{x})^2 - \frac{1}{2} G_N \int d^3x \int d^3y \frac{\rho(t, \bar{x}) \rho(t, \bar{y})}{|\bar{x} - \bar{y}|}, \end{aligned} \quad (4.1)$$

where on the first line we have point particles with masses m_i and positions \bar{x}_i , and on the second line we have gone over to a description in terms of a continuous fluid with density $\rho(t, \bar{x})$ and velocity \bar{v} . For a homogeneous and isotropic region with total mass $M = \frac{4\pi}{3} a(t)^3 \rho(t)$, where $a(t)$ is the radius, this reduces to [45] (page 86)

$$E = \frac{M}{10} a^2 \left(3 \frac{\dot{a}^2}{a^2} - 8\pi G_N \rho \right), \quad (4.2)$$

which is conserved. If we consider a dust FRW model with spatial curvature ${}^{(3)}R = -6K a^{-2}$, then (4.2) corresponds to the first Friedmann equation with the identification $E = -\frac{3}{10} M K$. So for this simple system, conservation of the Newtonian energy does correspond to the FRW spatial curvature evolving like $\propto a^{-2}$, in agreement with the above argument.

What about matter distribution that is not homogeneous and isotropic? With $\mathcal{Q} = 0$, the average Raychaudhuri equation (2.1) has (applying (2.3)) the same form as in the homogeneous and isotropic case.⁷ Therefore its first integral gives again the first Friedmann equation with a constant of integration like (4.2).⁸ In contrast, in the relativistic case, equation (2.2) that generalises the first Friedmann equation is an independent equation, and its integrability condition with (2.1) shows that in general $a^2 \langle {}^{(3)}R \rangle$ is not conserved, as $\mathcal{Q} \neq 0$. This corresponds to the fact that the conservation law for the spatial curvature in the relativistic FRW model is due to homogeneity and isotropy; in contrast the Newtonian case energy is conserved regardless of the symmetry (or lack of it) of the matter distribution. However, this energy explanation is limited in that conservation of the Newtonian energy does not, in fact, generally imply that backreaction vanishes, $\mathcal{Q} = 0$. For a single homogeneous non-spherical ellipsoid embedded in empty space, the Newtonian energy is conserved, but $\mathcal{Q} \neq 0$ (the variance is zero and the shear is non-zero). Another example is the union of two disjoint spherical regions. The energy of each region is conserved, so the total energy is also conserved, but $\mathcal{Q} \neq 0$, as energy is additive, but \mathcal{Q} is not [77, 78]. It is not clear whether

⁶See also [93] for a study of discrete Newtonian cosmology.

⁷The Raychaudhuri equation (2.1) is written for the relativistic case, but the Newtonian form is exactly the same.

⁸The equation (2.1) has the form of a Newtonian one-dimensional force law, so for any $\mathcal{Q} = \mathcal{Q}(a)$ it yields a conserved quantity. However, in general a non-zero \mathcal{Q} is not a function of the scale factor alone.

the Newtonian energy can always be associated with the conserved quantity coming from the Raychaudhuri equation in the cases when $\mathcal{Q} = 0$.

In some studies backreaction has been estimated by combining statistical modelling and Newtonian N -body simulation data in various degrees [29]. However, because backreaction on the expansion rate is zero for Newtonian gravity with periodic boundary conditions [14], non-zero backreaction is due to neglect of spherical asymmetry and/or proper matching of the regions to each other and the environment (see [92, 94] for recent discussion). While such studies may be useful in demonstrating timescales and orders of magnitude, there is limited information to be gained from any analysis that does not properly account for the difference between Newtonian and relativistic degrees of freedom and constraints in the non-linear regime.

5 Conclusions

The effect of structures. We have considered a statistical model for the effect of structure formation on the average expansion rate. We sample the initial Gaussian density field for ellipsoidal peaks and troughs with a time-dependent smoothing scale $R(t)$ determined by setting the root mean square density contrast to unity at all times, $\sigma_0(R, t) = 1$, so that we look at the generation of typical structures that is forming at each era. The peaks and troughs are modelled as homogeneous Newtonian ellipsoids, with the volume that is not in peaks and troughs taken to expand like the background. This extends the calculation of [33], where spherical regions were considered. We have also made other small improvements, like using spectral index $n = 0.96$ rather than the scale-invariant case, and using the numerical transfer function from CAMB. The ellipsoidal model allows us to estimate the contribution of the shear and the fraction of regions that have filamentary or planar structure. Our modelling does not properly capture the transfer of mass from underdense to overdense regions, so only half of the total mass is in overdense regions, in contrast to simulations and observations [40, 41]. Therefore filaments, sheets and clusters do not have a large effect in our calculation, the most important feature is the growth of the underdense regions.

Like the spherical case, the ellipsoidal case shows an increase of the expansion rate of the right order of magnitude, compared to observations, at late times. In the ellipsoidal case, Ht rises from the Einstein–de Sitter value $Ht = 2/3$, saturating at 0.83 around $t = 10^5$ Gyr. The shear slows down the expansion rate, so this is smaller than the spherical case value $Ht = 0.85$. This number is sensitive to the choice of smoothing scale. Changing the smoothing scale from $\sigma_0(R, t) = 1$ to 0.5 or 2 gives 0.74 or 0.88 as the asymptotic value. There is no acceleration, the expansion just decelerates more slowly. The change in the expansion rate is due to underdense regions expanding more rapidly than the background, so Ht is naturally between $2/3$ and the completely empty case value $Ht = 1$. The timing comes from the fact that the CDM transfer function rises around k_{eq} , so the number density of peaks and troughs grows when modes with $k \sim k_{\text{eq}}$ enter the non-linear regime. The timescale for this is determined by the matter-radiation equality time $t_{\text{eq}} = 5 \times 10^4$ yr and the small primordial perturbation amplitude $A = 5 \times 10^{-5}$ as $t \sim A^{-3/2} t_{\text{eq}} \sim 10^2$ Gyr.

Open questions. It is non-trivial that the right order of magnitude in the amplitude and roughly right timescale of the change in the expansion rate follow simply from the known physics of structure formation. However, the model has shortcomings that would need to be overcome for the results to be more than suggestive. All dimensionless quantities calculated from the ensemble are almost constant after structures with wavenumber k_{eq}

collapse, because the transfer function on those scales and the primordial spectrum are close to scale-invariant. However, as the expansion is faster than in the Einstein–de Sitter case, Ω_m should approach zero, not remain constant. This issue could be resolved with a more careful statistical treatment. A more difficult problem is whether the sampling of regions correctly reproduces the distinction between relativistic and Newtonian physics. This is a crucial question, given that backreaction is always small in a statistically homogeneous and isotropic universe in the Newtonian case, but not in general relativity [10, 14, 17]. Studies of backreaction that use data from Newtonian N -body simulations [29] face the same issue of how to relate the local Newtonian approximation to the global general relativistic setting. It remains to be seen whether this question can be answered via improved statistical models or if it will only be settled by relativistic cosmological simulations [30–32].

Acknowledgments

We thank Shaun Hotchkiss for contributing to this work.

References

- [1] W. B. Bonnor and G. F. R. Ellis, *Observational homogeneity of the universe*, *Mon. Not. Roy. Astron. Soc.* **218** (Feb., 1986) 605–614.
W. R. Stoeger, G. F. R. Ellis and C. Hellaby, *The relationship between continuum homogeneity and statistical homogeneity in cosmology*, *Mon. Not. Roy. Astron. Soc.* **226** (May, 1987) 373–381.
- [2] C. Clarkson and R. Maartens, *Inhomogeneity and the foundations of concordance cosmology*, *Class. Quant. Grav.* **27** (2010) 124008, [[1005.2165](#)].
A. F. Heavens, R. Jimenez and R. Maartens, *Testing homogeneity with the fossil record of galaxies*, *JCAP* **1109** (2011) 035, [[1107.5910](#)].
T. Clifton, C. Clarkson and P. Bull, *The isotropic blackbody CMB as evidence for a homogeneous universe*, *Phys. Rev. Lett.* **109** (2012) 051303, [[1111.3794](#)].
B. Hoyle, R. Tojeiro, R. Jimenez, A. Heavens, C. Clarkson and R. Maartens, *Testing homogeneity with galaxy star formation history*, *Astrophys. J.* **762** (2012) L9, [[1209.6181](#)].
- [3] D. W. Hogg, D. J. Eisenstein, M. R. Blanton, N. A. Bahcall, J. Brinkmann, J. E. Gunn et al., *Cosmic homogeneity demonstrated with luminous red galaxies*, *Astrophys. J.* **624** (2005) 54–58, [[astro-ph/0411197](#)].
F. S. Labini, *Characterizing the large scale inhomogeneity of the galaxy distribution*, *AIP Conf. Proc.* **1241** (2010) 981–990, [[0910.3833](#)].
F. S. Labini and L. Pietronero, *The complex universe: recent observations and theoretical challenges*, *J. Stat. Mech.* **1011** (2010) P11029, [[1012.5624](#)].
F. S. Labini, *Inhomogeneities in the universe*, *Class. Quant. Grav.* **28** (2011) 164003, [[1103.5974](#)].
F. S. Labini, *Very large scale correlations in the galaxy distribution*, *EPL* **96** (2011) 59001, [[1110.4041](#)].
M. Scrimgeour et al., *The WiggleZ Dark Energy Survey: the transition to large-scale cosmic homogeneity*, *Mon. Not. Roy. Astron. Soc.* **425** (2012) 116–134, [[1205.6812](#)].
S. Nadathur, *Seeing patterns in noise: Gigaparsec-scale ‘structures’ that do not violate homogeneity*, *Mon. Not. Roy. Astron. Soc.* **434** (2013) 398–406, [[1306.1700](#)].
F. S. Labini, D. Tekhanovich and Y. V. Baryshev, *Spatial density fluctuations and selection effects in galaxy redshift surveys*, *JCAP* **1407** (2014) 035, [[1406.5899](#)].
P. Laurent et al., *A $14\ h^{-3}\ Gpc^3$ study of cosmic homogeneity using BOSS DR12 quasar sample*, *JCAP* **1611** (2016) 060, [[1602.09010](#)].

- P. Ntelis et al., *Exploring cosmic homogeneity with the BOSS DR12 galaxy sample*, *JCAP* **1706** (2017) 019, [[1702.02159](#)].
- [4] S. Rasanen, *On the relation between the isotropy of the CMB and the geometry of the universe*, *Phys. Rev. D* **79** (2009) 123522, [[0903.3013](#)].
- [5] R. Maartens, *Is the Universe homogeneous?*, *Phil. Trans. Roy. Soc. Lond.* **A369** (2011) 5115–5137, [[1104.1300](#)].
- [6] G. F. R. Ellis, *Relativistic Cosmology: Its Nature, Aims and Problems*, *Fundam. Theor. Phys.* **9** (1984) 215–288.
G. F. R. Ellis and W. Stoeger, *The ‘fitting problem’ in cosmology*, *Class. Quant. Grav.* **4** (1987) 1697–1729.
- [7] G. F. R. Ellis and T. Buchert, *The Universe seen at different scales*, *Phys. Lett. A* **347** (2005) 38–46, [[gr-qc/0506106](#)].
- [8] S. Rasanen, *Backreaction: directions of progress*, *Class. Quant. Grav.* **28** (2011) 164008, [[1102.0408](#)].
- [9] T. Buchert and S. Räsänen, *Backreaction in late-time cosmology*, *Ann. Rev. Nucl. Part. Sci.* **62** (2012) 57–79, [[1112.5335](#)].
- [10] T. Buchert, *On average properties of inhomogeneous cosmologies*, in *Proceedings, 9th Workshop on General Relativity and Gravitation (JGRG9): Hiroshima, Japan, November 3-6, 1999*, 1999. [[gr-qc/0001056](#)].
- [11] C. Wetterich, *Can structure formation influence the cosmological evolution?*, *Phys. Rev. D* **67** (2003) 043513, [[astro-ph/0111166](#)].
- [12] D. J. Schwarz, *Accelerated expansion without dark energy*, in *18th IAP Colloquium on the Nature of Dark Energy: Observational and Theoretical Results on the Accelerating Universe Paris, France, July 1-5, 2002*, 2002. [[astro-ph/0209584](#)].
- [13] S. Rasanen, *Dark energy from backreaction*, *JCAP* **0402** (2004) 003, [[astro-ph/0311257](#)].
S. Rasanen, *Backreaction of linear perturbations and dark energy*, in *39th Rencontres de Moriond Workshop on Exploring the Universe: Contents and Structures of the Universe La Thuile, Italy, March 28-April 4, 2004*, 2004. [[astro-ph/0407317](#)].
- [14] T. Buchert and J. Ehlers, *Averaging inhomogeneous Newtonian cosmologies*, *Astron. Astrophys.* **320** (1997) 1–7, [[astro-ph/9510056](#)].
- [15] K. Enqvist, M. Mattsson and G. Rigopoulos, *Supernovae data and perturbative deviation from homogeneity*, *JCAP* **0909** (2009) 022, [[0907.4003](#)].
- [16] S. R. Green and R. M. Wald, *A new framework for analyzing the effects of small scale inhomogeneities in cosmology*, *Phys. Rev. D* **83** (2011) 084020, [[1011.4920](#)].
S. R. Green and R. M. Wald, *Examples of backreaction of small scale inhomogeneities in cosmology*, *Phys. Rev. D* **87** (2013) 124037, [[1304.2318](#)].
S. R. Green and R. M. Wald, *How well is our universe described by an FLRW model?*, *Class. Quant. Grav.* **31** (2014) 234003, [[1407.8084](#)].
T. Buchert et al., *Is there proof that backreaction of inhomogeneities is irrelevant in cosmology?*, *Class. Quant. Grav.* **32** (2015) 215021, [[1505.07800](#)].
S. R. Green and R. M. Wald, *Comments on Backreaction*, [[1506.06452](#)].
J. J. Ostrowski and B. F. Roukema, *On the Green and Wald formalism*, in *14th Marcel Grossmann Meeting on Recent Developments in Theoretical and Experimental General Relativity, Astrophysics, and Relativistic Field Theories (MG14) Rome, Italy, July 12-18, 2015*, 2015. [[1512.02947](#)].
S. R. Green and R. M. Wald, *A simple, heuristic derivation of our ‘no backreaction’ results*, *Class. Quant. Grav.* **33** (2016) 125027, [[1601.06789](#)].

- [17] M. Lavinto, S. Räsänen and S. J. Szybka, *Average expansion rate and light propagation in a cosmological Tardis spacetime*, *JCAP* **1312** (2013) 051, [[1308.6731](#)].
- [18] C. Clarkson, B. Bassett and T. H.-C. Lu, *A general test of the Copernican Principle*, *Phys. Rev. Lett.* **101** (2008) 011301, [[0712.3457](#)].
- [19] S. Räsänen, *A covariant treatment of cosmic parallax*, *JCAP* **1403** (2014) 035, [[1312.5738](#)].
- [20] S. Räsänen, K. Bolejko and A. Finoguenov, *New Test of the Friedmann-Lemaître-Robertson-Walker Metric Using the Distance Sum Rule*, *Phys. Rev. Lett.* **115** (2015) 101301, [[1412.4976](#)].
- [21] A. Shafieloo and C. Clarkson, *Model independent tests of the standard cosmological model*, *Phys. Rev.* **D81** (2010) 083537, [[0911.4858](#)].
E. Mortsell and J. Jonsson, *A model independent measure of the large scale curvature of the Universe*, **1102.4485**.
D. Sapone, E. Majerotto and S. Nesseris, *Curvature versus distances: Testing the FLRW cosmology*, *Phys. Rev.* **D90** (2014) 023012, [[1402.2236](#)].
R.-G. Cai, Z.-K. Guo and T. Yang, *Null test of the cosmic curvature using $H(z)$ and supernovae data*, *Phys. Rev.* **D93** (2016) 043517, [[1509.06283](#)].
B. L’Huillier and A. Shafieloo, *Model-independent test of the FLRW metric, the flatness of the Universe, and non-local measurement of H_{0rd}* , *JCAP* **1701** (2017) 015, [[1606.06832](#)].
H. Yu and F. Y. Wang, *New model-independent method to test the curvature of the universe*, *Astrophys. J.* **828** (2016) 85, [[1605.02483](#)].
Z. Li, G.-J. Wang, K. Liao and Z.-H. Zhu, *Model-independent estimations for the curvature from standard candles and clocks*, *Astrophys. J.* **833** (2016) 240, [[1611.00359](#)].
J.-J. Wei and X.-F. Wu, *An Improved Method to Measure the Cosmic Curvature*, *Astrophys. J.* **838** (2017) 160, [[1611.00904](#)].
F. Montanari and S. Rasanen, *Backreaction and FRW consistency conditions*, **1709.06022**.
- [22] C. Boehm and S. Räsänen, *Violation of the FRW consistency condition as a signature of backreaction*, *JCAP* **1309** (2013) 003, [[1305.7139](#)].
- [23] S. Rasanen, *Light propagation in statistically homogeneous and isotropic dust universes*, *JCAP* **0902** (2009) 011, [[0812.2872](#)].
- [24] S. Rasanen, *Light propagation in statistically homogeneous and isotropic universes with general matter content*, *JCAP* **1003** (2010) 018, [[0912.3370](#)].
- [25] C. Clarkson, G. F. R. Ellis, A. Faltenbacher, R. Maartens, O. Umeh and J.-P. Uzan, *(Mis-)Interpreting supernovae observations in a lumpy universe*, *Mon. Not. Roy. Astron. Soc.* **426** (2012) 1121–1136, [[1109.2484](#)].
- [26] P. Bull and T. Clifton, *Local and non-local measures of acceleration in cosmology*, *Phys. Rev.* **D85** (2012) 103512, [[1203.4479](#)].
- [27] T. Clifton and P. G. Ferreira, *Archipelagian Cosmology: Dynamics and Observables in a Universe with Discretized Matter Content*, *Phys. Rev.* **D80** (2009) 103503, [[0907.4109](#)].
T. Clifton and P. G. Ferreira, *Errors in Estimating Ω_Λ due to the Fluid Approximation*, *JCAP* **0910** (2009) 026, [[0908.4488](#)].
T. Clifton, K. Rosquist and R. Tavakol, *An Exact quantification of backreaction in relativistic cosmology*, *Phys. Rev.* **D86** (2012) 043506, [[1203.6478](#)].
T. Clifton, *Cosmology Without Averaging*, *Class. Quant. Grav.* **28** (2011) 164011, [[1005.0788](#)].
T. Clifton, P. G. Ferreira and K. O’Donnell, *An Improved Treatment of Optics in the Lindquist-Wheeler Models*, *Phys. Rev.* **D85** (2012) 023502, [[1110.3191](#)].
T. Clifton, D. Gregoris, K. Rosquist and R. Tavakol, *Exact Evolution of Discrete Relativistic Cosmological Models*, *JCAP* **1311** (2013) 010, [[1309.2876](#)].
T. Clifton, D. Gregoris and K. Rosquist, *Piecewise Silence in Discrete Cosmological Models*, *Class. Quant. Grav.* **31** (2014) 105012, [[1402.3201](#)].

- T. Clifton, *The Method of Images in Cosmology*, *Class. Quant. Grav.* **31** (2014) 175010, [[1405.3197](#)].
- V. A. A. Sanghai and T. Clifton, *Post-Newtonian Cosmological Modelling*, *Phys. Rev.* **D91** (2015) 103532, [[1503.08747](#)].
- T. Clifton, *What's the Matter in Cosmology?*, 2015. [[1509.06682](#)].
- V. A. A. Sanghai and T. Clifton, *Cosmological backreaction in the presence of radiation and a cosmological constant*, *Phys. Rev.* **D94** (2016) 023505, [[1604.06345](#)].
- J. Durk and T. Clifton, *Exact Initial Data for Black Hole Universes with a Cosmological Constant*, *Class. Quant. Grav.* **34** (2017) 065009, [[1610.05635](#)].
- R. Bibi, T. Clifton and J. Durk, *Cosmological Solutions with Charged Black Holes*, *Gen. Rel. Grav.* **49** (2017) 98, [[1705.01892](#)].
- J. Durk and T. Clifton, *A Quasi-Static Approach to Structure Formation in Black Hole Universes*, [[1707.08056](#)].
- [28] T. Clifton, D. Gregoris and K. Rosquist, *The Magnetic Part of the Weyl Tensor, and the Expansion of Discrete Universes*, *Gen. Rel. Grav.* **49** (2017) 30, [[1607.00775](#)].
- [29] A. Wiegand and T. Buchert, *Multi-scale cosmology and structure-emerging Dark Energy: a plausibility analysis*, *Phys. Rev.* **D82** (2010) 023523, [[1002.3912](#)].
- A. Wiegand and T. Buchert, *Multiscale approach to inhomogeneous cosmologies*, *J. Cosmol.* **15** (2011) 6100, [[1103.1531](#)].
- B. F. Roukema, J. J. Ostrowski and T. Buchert, *Virialisation-induced curvature as a physical explanation for dark energy*, *JCAP* **1310** (2013) 043, [[1303.4444](#)].
- G. Racz, L. Dobos, R. Beck, I. Szapudi and I. Csabai, *Concordance cosmology without dark energy*, *Mon. Not. Roy. Astron. Soc.* **469** (2017) L1–L5, [[1607.08797](#)].
- B. F. Roukema, *Replacing dark energy by silent virialisation*, [[1706.06179](#)].
- [30] J. Adamek, D. Daverio, R. Durrer and M. Kunz, *General Relativistic N-body simulations in the weak field limit*, *Phys. Rev.* **D88** (2013) 103527, [[1308.6524](#)].
- J. Adamek, C. Clarkson, R. Durrer and M. Kunz, *Does small scale structure significantly affect cosmological dynamics?*, *Phys. Rev. Lett.* **114** (2015) 051302, [[1408.2741](#)].
- J. Adamek, R. Durrer and M. Kunz, *N-body methods for relativistic cosmology*, *Class. Quant. Grav.* **31** (2014) 234006, [[1408.3352](#)].
- J. Adamek, D. Daverio, R. Durrer and M. Kunz, *General relativity and cosmic structure formation*, *Nature Phys.* **12** (2016) 346–349, [[1509.01699](#)].
- J. Adamek, D. Daverio, R. Durrer and M. Kunz, *gevolution: a cosmological N-body code based on General Relativity*, *JCAP* **1607** (2016) 053, [[1604.06065](#)].
- [31] C.-M. Yoo, H. Abe, K.-i. Nakao and Y. Takamori, *Black Hole Universe: Construction and Analysis of Initial Data*, *Phys. Rev.* **D86** (2012) 044027, [[1204.2411](#)].
- E. Bentivegna and M. Korzynski, *Evolution of a periodic eight-black-hole lattice in numerical relativity*, *Class. Quant. Grav.* **29** (2012) 165007, [[1204.3568](#)].
- E. Bentivegna, *Black-hole lattices*, *Springer Proc. Math. Stat.* **60** (2014) 143–146, [[1307.7673](#)].
- J. Adamek, M. Gosenca and S. Hotchkiss, *Spherically Symmetric N-body Simulations with General Relativistic Dynamics*, *Phys. Rev.* **D93** (2016) 023526, [[1509.01163](#)].
- E. Bentivegna, M. Korzyński, I. Hinder and D. Gerlicher, *Light propagation through black-hole lattices*, *JCAP* **1703** (2017) 014, [[1611.09275](#)].
- [32] E. Bentivegna and M. Bruni, *Effects of nonlinear inhomogeneity on the cosmic expansion with numerical relativity*, *Phys. Rev. Lett.* **116** (2016) 251302, [[1511.05124](#)].
- J. T. Giblin, J. B. Mertens and G. D. Starkman, *Departures from the Friedmann-Lemaître-Robertson-Walker Cosmological Model in an Inhomogeneous Universe: A Numerical Examination*, *Phys. Rev. Lett.* **116** (2016) 251301, [[1511.01105](#)].
- J. B. Mertens, J. T. Giblin and G. D. Starkman, *Integration of inhomogeneous cosmological spacetimes in the BSSN formalism*, *Phys. Rev.* **D93** (2016) 124059, [[1511.01106](#)].
- H. J. Macpherson, P. D. Lasky and D. J. Price, *Inhomogeneous Cosmology with Numerical*

- Relativity*, *Phys. Rev.* **D95** (2017) 064028, [[1611.05447](#)].
- J. T. Giblin, J. B. Mertens and G. D. Starkman, *A cosmologically motivated reference formulation of numerical relativity*, [1704.04307](#).
- [33] S. Rasanen, *Evaluating backreaction with the peak model of structure formation*, *JCAP* **0804** (2008) 026, [[0801.2692](#)].
 - [34] S. F. Shandarin and A. A. Klypin, *Rich Galaxy Clusters may Result from Largescale Motions Inside Superclusters*, *Soviet Astronomy* **28** (Oct., 1984) 491–495.
 - [35] N. Katz, T. Quinn and J. M. Gelb, *Galaxy Formation and the Peaks Formalism*, *Mon. Not. Roy. Astron. Soc.* **265** (Dec., 1993) 689.
 - [36] R. van de Weygaert and A. Babul, *Shear fields and the evolution of galactic scale density peaks*, *Astrophys. J.* **425** (1994) L59, [[astro-ph/9402003](#)].
 - [37] L. Kofman and D. Pogosian, *Equations of gravitational instability are nonlocal*, *Astrophys. J.* **442** (1995) 30–38, [[astro-ph/9403029](#)].
 - [38] C. Porciani, A. Dekel and Y. Hoffman, *Testing tidal-torque theory. 2. Alignment of inertia and shear and the characteristics of proto-haloes*, *Mon. Not. Roy. Astron. Soc.* **332** (2002) 339, [[astro-ph/0105165](#)].
 - [39] A. D. Ludlow and C. Porciani, *The Peaks Formalism and the Formation of Cold Dark Matter Haloes*, *Mon. Not. Roy. Astron. Soc.* **413** (2011) 1961–1972, [[1011.2493](#)].
 - [40] J. R. Bond, L. Kofman and D. Pogosyan, *How filaments are woven into the cosmic web*, *Nature* **380** (1996) 603–606, [[astro-ph/9512141](#)].
 - [41] M. Cautun, R. van de Weygaert, B. J. T. Jones and C. S. Frenk, *Evolution of the cosmic web*, *Mon. Not. Roy. Astron. Soc.* **441** (2014) 2923–2973, [[1401.7866](#)].
 - [42] Y. B. Zel’dovich, *Gravitational instability: An approximate theory for large density perturbations.*, *Astronomy and Astrophysics* **D 5** (Mar., 1970) 84–89.
 - [43] V. Icke, *Formation of Galaxies inside Clusters*, *Astronomy and Astrophysics* **D 27** (Aug., 1973) 1.
 - [44] S. D. M. White and J. Silk, *The growth of aspherical structure in the universe - Is the local supercluster an unusual system*, *Astrophys. J.* **231** (July, 1979) 1–9.
 - [45] P. J. E. Peebles and G. Shaviv, *The Large-Scale Structure of the Universe*, *Space Science Reviews* **31** (Mar., 1982) 119.
 - [46] Y. Hoffman, *The dynamics of superclusters - The effect of shear*, *Astrophys. J.* **308** (Sept., 1986) 493–498.
 - [47] D. J. Eisenstein and A. Loeb, *An Analytical model for the triaxial collapse of cosmological perturbations*, *Astrophys. J.* **439** (1995) 520, [[astro-ph/9405012](#)].
 - [48] R. van de Weygaert and E. Bertschinger, *Constraining peaks in Gaussian primordial density fields: an application of the hoffman-ribak method*, *Mon. Not. Roy. Astron. Soc.* **281** (1996) 84, [[astro-ph/9507024](#)].
 - [49] E. Audit and J.-M. Alimi, *Gravitational Lagrangian dynamics of cold matter using the deformation tensor*, *Astron. Astrophys.* **315** (1996) 11–20, [[astro-ph/9609156](#)].
 - [50] J. R. Bond and S. T. Myers, *The Peak-Patch Picture of Cosmic Catalogs. I. Algorithms*, *Astrophys. J. Suppl.* **103** (Mar., 1996) 1.
 - [51] A. Del Popolo, E. N. Ercan and Z. Xia, *Ellipsoidal collapse and previrialization*, *Astron. J.* **122** (2001) 487–495, [[astro-ph/0108080](#)].
 - [52] A. D. Popolo, *On the evolution of aspherical perturbations in the universe: an analytical model*, *Astron. Astrophys.* **387** (2002) 759, [[astro-ph/0202436](#)].

- [53] R. K. Sheth, H. J. Mo and G. Tormen, *Ellipsoidal collapse and an improved model for the number and spatial distribution of dark matter haloes*, *Mon. Not. Roy. Astron. Soc.* **323** (2001) 1, [[astro-ph/9907024](#)].
- [54] R. K. Sheth and G. Tormen, *An Excursion set model of hierarchical clustering : Ellipsoidal collapse and the moving barrier*, *Mon. Not. Roy. Astron. Soc.* **329** (2002) 61, [[astro-ph/0105113](#)].
- [55] Y. Ohta, I. Kayo and A. Taruya, *Evolution of cosmological density distribution function from the local collapse model*, *Astrophys. J.* **589** (2003) 1–16, [[astro-ph/0301567](#)].
- [56] Y. Ohta, I. Kayo and A. Taruya, *Cosmological density distribution function from the ellipsoidal collapse model in real space*, *Astrophys. J.* **608** (2004) 647–662, [[astro-ph/0402618](#)].
- [57] T. Y. Lam and R. K. Sheth, *Ellipsoidal collapse and the redshift space probability distribution function of dark matter*, *Mon. Not. Roy. Astron. Soc.* **389** (2008) 1249, [[0805.1238](#)].
- [58] B. E. Robertson, A. V. Kravtsov, J. Tinker and A. R. Zentner, *Collapse Barriers and Halo Abundance: Testing the Excursion Set Ansatz*, *Astrophys. J.* **696** (2009) 636–652, [[0812.3148](#)].
- [59] C. Angrick and M. Bartelmann, *Triaxial collapse and virialisation of dark-matter haloes*, *Astron. Astrophys.* **518** (2010) A38, [[1001.4984](#)].
- [60] A. D. Ludlow, C. Porciani and M. Borzyszkowski, *The formation of CDM haloes – I. Collapse thresholds and the ellipsoidal collapse model*, *Mon. Not. Roy. Astron. Soc.* **445** (2014) 4110–4123, [[1107.5808](#)].
- [61] A. Paranjape and R. K. Sheth, *Peaks theory and the excursion set approach*, *Mon. Not. Roy. Astron. Soc.* **426** (2012) 2789–2796, [[1206.3506](#)].
- [62] A. Paranjape, R. K. Sheth and V. Desjacques, *Excursion set peaks: a self-consistent model of dark halo abundances and clustering*, *Mon. Not. Roy. Astron. Soc.* **431** (2013) 1503–1512, [[1210.1483](#)].
- [63] R. Reischke, F. Pace, S. Meyer and B. M. Schäfer, *Spherical collapse of dark matter haloes in tidal gravitational fields*, *Mon. Not. Roy. Astron. Soc.* **463** (2016) 429–440, [[1606.09207](#)].
- [64] T. Buchert, M. Kerscher and C. Sicka, *Back reaction of inhomogeneities on the expansion: The Evolution of cosmological parameters*, *Phys. Rev.* **D62** (2000) 043525, [[astro-ph/9912347](#)].
- [65] C.-H. Chuang, J.-A. Gu and W.-Y. P. Hwang, *Inhomogeneity-induced cosmic acceleration in a dust universe*, *Class. Quant. Grav.* **25** (2008) 175001, [[astro-ph/0512651](#)].
A. Paranjape and T. P. Singh, *The Possibility of Cosmic Acceleration via Spatial Averaging in Lemaitre-Tolman-Bondi Models*, *Class. Quant. Grav.* **23** (2006) 6955–6969, [[astro-ph/0605195](#)].
- [66] T. Kai, H. Kozaki, K.-i. nakao, Y. Nambu and C.-M. Yoo, *Can inhomogeneties accelerate the cosmic volume expansion?*, *Prog. Theor. Phys.* **117** (2007) 229–240, [[gr-qc/0605120](#)].
- [67] T. Buchert, *On average properties of inhomogeneous fluids in general relativity. 1. Dust cosmologies*, *Gen. Rel. Grav.* **32** (2000) 105–125, [[gr-qc/9906015](#)].
- [68] T. Buchert, *On average properties of inhomogeneous fluids in general relativity: Perfect fluid cosmologies*, *Gen. Rel. Grav.* **33** (2001) 1381–1405, [[gr-qc/0102049](#)].
- [69] J. Larena, *Spatially averaged cosmology in an arbitrary coordinate system*, *Phys. Rev.* **D79** (2009) 084006, [[0902.3159](#)].
- [70] D. D. Malament, *Is Newtonian cosmology really inconsistent?*, *Philosophy of Science* **62** (1995) 489.
J. D. Norton, *The force of Newtonian cosmology: acceleration is relative*, *Philosophy of Science* **62** (1995) 511.

- [71] PLANCK collaboration, P. A. R. Ade et al., *Planck 2015 results. XIII. Cosmological parameters*, *Astron. Astrophys.* **594** (2016) A13, [[1502.01589](#)].
- [72] J. M. Bardeen, J. R. Bond, N. Kaiser and A. S. Szalay, *The statistics of peaks of Gaussian random fields*, *Astrophys. J.* **304** (May, 1986) 15–61.
- [73] A. G. Doroshkevich, *The space structure of perturbations and the origin of rotation of galaxies in the theory of fluctuation.*, *Astrofizika* **6** (1970) 581–600.
- [74] C. Angrick, *Ellipticity and prolativity of the initial gravitational-shear field at the position of density maxima*, *Mon. Not. Roy. Astron. Soc.* **443** (2014) 2361–2371, [[1305.0497](#)].
- [75] A. Lewis, A. Challinor and A. Lasenby, *Efficient computation of CMB anisotropies in closed FRW models*, *Astrophys. J.* **538** (2000) 473–476, [[astro-ph/9911177](#)].
- [76] M. Vonlanthen, S. Rasanen and R. Durrer, *Model-independent cosmological constraints from the CMB*, *JCAP* **1008** (2010) 023, [[1003.0810](#)].
 B. Audren, J. Lesgourgues, K. Benabed and S. Prunet, *Conservative Constraints on Early Cosmology: an illustration of the Monte Python cosmological parameter inference code*, *JCAP* **1302** (2013) 001, [[1210.7183](#)].
 B. Audren, *Separate Constraints on Early and Late Cosmology*, *Mon. Not. Roy. Astron. Soc.* **444** (2014) 827–832, [[1312.5696](#)].
- [77] S. Rasanen, *Cosmological acceleration from structure formation*, *Int. J. Mod. Phys. D* **15** (2006) 2141–2146, [[astro-ph/0605632](#)].
- [78] S. Rasanen, *Accelerated expansion from structure formation*, *JCAP* **0611** (2006) 003, [[astro-ph/0607626](#)].
- [79] C. Shapiro and M. S. Turner, *What do we really know about cosmic acceleration?*, *Astrophys. J.* **649** (2006) 563–569, [[astro-ph/0512586](#)].
 Y. Gong and A. Wang, *Observational constraints on the acceleration of the universe*, *Phys. Rev. D* **73** (2006) 083506, [[astro-ph/0601453](#)].
 O. Elgaroy and T. Multamaki, *Bayesian analysis of friedmannless cosmologies*, *JCAP* **0609** (2006) 002, [[astro-ph/0603053](#)].
 M. Seikel and D. J. Schwarz, *How strong is the evidence for accelerated expansion?*, *JCAP* **0802** (2008) 007, [[0711.3180](#)].
 M. Seikel and D. J. Schwarz, *Model- and calibration-independent test of cosmic acceleration*, *JCAP* **0902** (2009) 024, [[0810.4484](#)].
 E. Mortsell and C. Clarkson, *Model independent constraints on the cosmological expansion rate*, *JCAP* **0901** (2009) 044, [[0811.0981](#)].
 A. C. C. Guimaraes, J. V. Cunha and J. A. S. Lima, *Bayesian Analysis and Constraints on Kinematic Models from Union SNIa*, *JCAP* **0910** (2009) 010, [[0904.3550](#)].
 P. Serra, A. Cooray, D. E. Holz, A. Melchiorri, S. Pandolfi and D. Sarkar, *No Evidence for Dark Energy Dynamics from a Global Analysis of Cosmological Data*, *Phys. Rev. D* **80** (2009) 121302, [[0908.3186](#)].
 R.-G. Cai, Q. Su and H.-B. Zhang, *Probing the dynamical behavior of dark energy*, *JCAP* **1004** (2010) 012, [[1001.2207](#)].
 S. Wang, X.-D. Li and M. Li, *Exploring the Latest Union2 SNIa Dataset by Using Model-Independent Parametrization Methods*, *Phys. Rev. D* **83** (2011) 023010, [[1009.5837](#)].
 J. Park, C.-G. Park and J.-c. Hwang, *Analysis of recent type Ia supernova data based on evolving dark energy models*, *Phys. Rev. D* **84** (2011) 023506, [[1011.1723](#)].
 A. V. Pan and U. Alam, *Reconstructing Dark Energy : A Comparison of Cosmological Parameters*, **1012.1591**.
 R.-G. Cai and Z.-L. Tuo, *Detecting the cosmic acceleration with current data*, *Phys. Lett. B* **706** (2011) 116–122, [[1105.1603](#)].
 X.-D. Li, S. Li, S. Wang, W.-S. Zhang, Q.-G. Huang and M. Li, *Probing Cosmic Acceleration by Using the SNLS3 SNIa Dataset*, *JCAP* **1107** (2011) 011, [[1106.4116](#)].

- A. Shafieloo, A. G. Kim and E. V. Linder, *Gaussian Process Cosmography*, *Phys. Rev.* **D85** (2012) 123530, [[1204.2272](#)].
- A. Aviles, C. Gruber, O. Luongo and H. Quevedo, *Cosmography and constraints on the equation of state of the Universe in various parametrizations*, *Phys. Rev.* **D86** (2012) 123516, [[1204.2007](#)].
- J. Magaña, V. H. Cárdenas and V. Motta, *Cosmic slowing down of acceleration for several dark energy parametrizations*, *JCAP* **1410** (2014) 017, [[1407.1632](#)].
- Q.-G. Huang and K. Wang, *How the dark energy can reconcile Planck with local determination of the Hubble constant*, *Eur. Phys. J.* **C76** (2016) 506, [[1606.05965](#)].
- PLANCK collaboration, P. A. R. Ade et al., *Planck 2015 results. XIV. Dark energy and modified gravity*, *Astron. Astrophys.* **594** (2016) A14, [[1502.01590](#)].
- [80] C. Cattoen and M. Visser, *Cosmography: Extracting the Hubble series from the supernova data*, [gr-qc/0703122](#).
M. Visser and C. Cattoen, *Cosmographic analysis of dark energy*, in *Proceedings, 7th International Heidelberg Conference on Dark Matter in Astro and Particle Physics (DARK 2009): Christchurch, New Zealand, January 18-24, 2009*, pp. 287–300, 2009. [0906.5407](#). DOI.
- [81] C. Clarkson, T. Clifton, A. Coley and R. Sung, *Observational Constraints on the Averaged Universe*, *Phys. Rev.* **D85** (2012) 043506, [[1111.2214](#)].
- [82] P. M. Okouma, Y. Fantaye and B. A. Bassett, *How Flat is Our Universe Really?*, *Phys. Lett.* **B719** (2013) 1–4, [[1207.3000](#)].
- [83] B. R. Zhang, M. J. Childress, T. M. Davis, N. V. Karpenka, C. Lidman, B. P. Schmidt et al., *A blinded determination of H_0 from low-redshift Type Ia supernovae, calibrated by Cepheid variables*, [1706.07573](#).
- [84] G. Efstathiou, *H_0 Revisited*, *Mon. Not. Roy. Astron. Soc.* **440** (2014) 1138–1152, [[1311.3461](#)].
A. G. Riess et al., *A 2.4% Determination of the Local Value of the Hubble Constant*, *Astrophys. J.* **826** (2016) 56, [[1604.01424](#)].
W. Cardona, M. Kunz and V. Pettorino, *Determining H_0 with Bayesian hyper-parameters*, *JCAP* **1703** (2017) 056, [[1611.06088](#)].
B. Follin and L. Knox, *Insensitivity of The Distance Ladder Hubble Constant Determination to Cepheid Calibration Modeling Choices*, [1707.01175](#).
S. M. Feeney, D. J. Mortlock and N. Dalmaso, *Clarifying the Hubble constant tension with a Bayesian hierarchical model of the local distance ladder*, [1707.00007](#).
- [85] L. M. Krauss and B. Chaboyer, *Age Estimates of Globular Clusters in the Milky Way: Constraints on Cosmology*, *Science* **299** (Jan., 2003) 65–70.
- [86] S. Hofmann, D. J. Schwarz and H. Stoecker, *Formation of small-scale structure in SUSY CDM*, in *Proceedings, 4th International Workshop on The identification of dark matter (IDM 2002): York, UK, September 2-6, 2002*, pp. 45–51, 2002. [astro-ph/0211325](#). DOI.
A. M. Green, S. Hofmann and D. J. Schwarz, *The power spectrum of SUSY - CDM on sub-galactic scales*, *Mon. Not. Roy. Astron. Soc.* **353** (2004) L23, [[astro-ph/0309621](#)].
A. M. Green, S. Hofmann and D. J. Schwarz, *The First wimpy halos*, *JCAP* **0508** (2005) 003, [[astro-ph/0503387](#)].
A. M. Green, S. Hofmann and D. J. Schwarz, *Small scale wimp physics*, *AIP Conf. Proc.* **805** (2006) 431–434, [[astro-ph/0508553](#)].
- [87] P. Szekeres, *A class of inhomogeneous cosmological models*, *Communications in Mathematical Physics* **41** (Feb., 1975) 55–64.
- [88] R. Reischke, F. Pace, S. Meyer and B. M. Schafer, *Shear and vorticity in the spherical collapse of dark matter haloes*, [1612.04275](#).
- [89] H. van Elst, C. Uggla, W. M. Lesame, G. F. R. Ellis and R. Maartens, *Integrability of*

- irrotational silent cosmological models*, *Class. Quant. Grav.* **14** (1997) 1151–1162, [[gr-qc/9611002](#)].
- C. F. Sopuerta, *New study of silent universes*, *Phys. Rev. D* **55** (May, 1997) 5936–5950.
- [90] G. F. R. Ellis, *Relativistic cosmology*, *Gen. Rel. Grav.* **41** (2009) 581–660.
- G. F. R. Ellis and P. K. S. Dunsby, *Newtonian evolution of the Weyl tensor*, *Astrophys. J.* **479** (1997) 97, [[astro-ph/9410001](#)].
- S. Matarrese and D. Terranova, *PostNewtonian cosmological dynamics in Lagrangian coordinates*, *Mon. Not. Roy. Astron. Soc.* **283** (1996) 400–418, [[astro-ph/9511093](#)].
- H. van Elst and G. F. R. Ellis, *QuasiNewtonian dust cosmologies*, *Class. Quant. Grav.* **15** (1998) 3545–3573, [[gr-qc/9805087](#)].
- J. Ehlers, *Examples of Newtonian limits of relativistic spacetimes*, *Classical and Quantum Gravity* **14** (Jan., 1997) A119–A126.
- J. Ehlers and T. Buchert, *On the Newtonian Limit of the Weyl Tensor*, *Gen. Rel. Grav.* **41** (2009) 2153–2158, [[0907.2645](#)].
- [91] S. Rasanen, *Light propagation and the average expansion rate in near-FRW universes*, *Phys. Rev. D* **85** (2012) 083528, [[1107.1176](#)].
- [92] T. Buchert, *Comment on: "Why there is no Newtonian backreaction" by N. Kaiser*, [[1704.00703](#)].
- [93] G. F. R. Ellis and G. W. Gibbons, *Discrete Newtonian Cosmology*, *Class. Quant. Grav.* **31** (2014) 025003, [[1308.1852](#)].
- [94] N. Kaiser, *Why there is no Newtonian backreaction*, *Mon. Not. Roy. Astron. Soc.* **469** (2017) 744–748, [[1703.08809](#)].